Competitive and Cooperative Effects of Chloride on Palladium(II) Adsorption to Iron (Oxyhydr)oxides: Implications for Mobility During Weathering

Emily G. Wright[1], Xicheng He[2], Elaine D. Flynn[1], Daniel E. Giammar[2], Jeffrey G. Catalano[1*]

[1]Department of Earth, Environmental, and Planetary Sciences, Washington University in St. Louis, Saint Louis, MO 63130, USA

[2]Department of Energy, Environmental, and Chemical Engineering, Washington University in St. Louis, Saint Louis, MO 63130, USA

*Corresponding author: catalano@wustl.edu

Submitted to *Geochimica et Cosmochimica Acta*
September 2024

ABSTRACT

In surface and near-surface weathering environments, the mobilization and partial loss of palladium (Pd) under oxidizing and weakly acidic conditions has been attributed to aqueous chloride complexation. However, prior work has also observed that a portion of Pd is retained by iron (oxyhydr)oxides in the weathering zone. The effect chloride has on the relative amount of Pd mobilization versus retention by iron (oxyhydr)oxides is currently unclear. We studied the effect of chloride complexation on Pd(II) adsorption to two iron (oxyhydr)oxides, hematite and 2-line ferrihydrite, at pH 4. Increasing chloride concentration suppresses Pd adsorption for both hematite and ferrihydrite, which display similar binding affinities under the conditions studied. Thermodynamic modeling of aqueous Pd speciation indicates that greater suppression of binding to iron (oxyhydr)oxides should occur than is observed because of the strength of Pd-Cl complexation, implying that additional interactions at the mineral surface are counteracting this effect. While increasing dissolved chloride concentration does not measurably impact mineral surface charging, extended X-ray absorption fine structure (EXAFS) spectra indicate that ternary Pd-Cl surface complexes form on both hematite and ferrihydrite. The number of Cl ligands in the surface species increase at greater chloride concentration. A mixture of bidentate and monodentate surface species are indicated by the EXAFS spectra, although the fitting uncertainties precludes determining whether these vary in relative abundance with chloride concentration. In order to offset the effect of strong aqueous Pd-Cl complexation and align with our EXAFS results, a surface complexation model developed for Pd adsorption to hematite involves a mixture of three ternary surface complexes containing 1, 2, and 3 chloride ligands. Our results show that Pd is mobilized as a chloride complex in platinum group element-rich

weathering zones. Porewater chloride concentrations are thus a dominant control on Pd retention by iron (oxyhydr)oxides in these weakly acidic environments.

Keywords: Adsorption, Palladium, Iron oxides, Weathering

1. INTRODUCTION

The platinum-group elements (PGEs) are vital to many industrial applications yet are rare in the natural environment, concentrated and mined mostly in a few magmatic sulfide deposits (Zientek et al., 2017). The vulnerability of the PGE supply chain has led to them recently being designated as critical minerals (Nassar and Fortier, 2021). One potential resource to meet demand for PGEs are weathering zones that develop above ultramafic rock, including the oxidized zones that overlie world-class PGE deposits (Evans and Spratt, 2000; Evans, 2002; Oberthür and Melcher, 2005; Oberthür et al., 2013; Becker et al., 2014; Kraemer et al., 2017; Sefako et al., 2019; Dzingai et al., 2021). However, the fundamental processes that control the distribution and mobility of PGEs broadly, and palladium (Pd) more specifically, during oxic weathering are poorly constrained.

Palladium is primarily mined from reef, conduit, and contact-type deposits that are associated with large igneous intrusions, although several other types of deposits also contain elevated levels of PGEs, including hydrothermal and sedimentary deposits (Pašava, 1993; Wilde, 2005; Zientek et al., 2017). Recent work has focused on oxide-rich deposits formed by the weathering of mafic and ultramafic rock. These deposits include both the zones that develop above world-class PGE deposits (Evans et al., 1994; Hey, 1999; Evans and Spratt, 2000; Oberthür et al., 2000; Stribrny et al., 2000; Oberthür et al., 2003; Oberthür and Melcher, 2005;

87 Locmelis et al., 2010; Oberthür, 2018; Junge et al., 2019) and other laterites that develop above
88 ultramafic rocks that are not substantially enriched in PGEs (Traoré et al., 2006; Ndjigui et al.,
89 2008; Ndjigui and Bilong, 2010; Suárez et al., 2010; Aiglsperger et al., 2014; Oppermann et al.,
90 2017; Al-Khirbash and Ahmed, 2021; Ito et al., 2021). Weathering zones may be a substantial
91 future source of PGEs, with oxidized ores from the Great Dyke deposit in Zimbabwe alone
92 having estimated total resources of up to 250 Mt (Oberthür et al., 2013). Even in laterites that are
93 not associated with a PGE-rich intrusion, Pd concentrations are far in excess of the estimated
94 average upper continental crustal abundance of 0.8 μg/kg (Traoré et al., 2006; Ndjigui et al.,
95 2008; Ndjigui and Bilong, 2010; Suárez et al., 2010; Aiglsperger et al., 2014; Chen et al., 2016;
96 Oppermann et al., 2017; Al-Khirbash and Ahmed, 2021; Ito et al., 2021). Weathering zones thus
97 represent a promising resource for PGEs (Zientek et al., 2017). However, processes during
98 weathering result in PGEs being redistributed among different minerals (particularly oxides) and
99 displaying distinct depletion patterns not observed in primary deposits (Fuchs and Rose, 1974;
100 Evans et al., 1994; Hey, 1999; Evans and Spratt, 2000; Oberthür et al., 2000; Stribrny et al.,
101 2000; Oberthür et al., 2003; Oberthür and Melcher, 2005; Traoré et al., 2006; Ndjigui et al.,
102 2008; Locmelis et al., 2010; Ndjigui and Bilong, 2010; Suárez et al., 2010; Oberthür et al., 2013;
103 Oppermann et al., 2017; Oberthür, 2018; Junge et al., 2019; Ito et al., 2021).
104 In oxidized weathering zones, Pd is frequently associated with secondary iron
105 (oxyhydr)oxides at concentrations of up to 3,100 mg/kg (Oberthür et al., 2003; Oberthür and
106 Melcher, 2005; Locmelis et al., 2010; Suárez et al., 2010; Oberthür et al., 2013; Becker et al.,
107 2014; Oberthür, 2018; Junge et al., 2019). While Pd is also associated with several alteration
108 phases in these weathering zones (Evans et al., 1994; Evans and Spratt, 2000; Oberthür et al.,
109 2003; Oberthür and Melcher, 2005; Locmelis et al., 2010; Suárez et al., 2010; Oberthür et al.,

2013; Oberthür, 2018; Junge et al., 2019), iron (oxyhydr)oxides are one of the major weathering products by volume and a key reactive mineral in laterites (Marsh and Anderson, 2011). Despite this relative enrichment in iron (oxyhydr)oxides, Pd also shows greater mobility in these deposits compared to platinum (Pt) and appears to be preferentially lost during weathering (Fuchs and Rose, 1974; Evans et al., 1994; Oberthür et al., 2003; Oberthür and Melcher, 2005; Traoré et al., 2006; Ndjigui et al., 2008; Locmelis et al., 2010; Suárez et al., 2010; Ito et al., 2021). Aqueous chloride complexation under weakly acidic, oxidizing conditions is hypothesized to be responsible for this difference in mobility (Fuchs and Rose, 1974); Pd forms strong aqueous complexes with chloride while chloride complexation with Pt dominates only at very low pH (Wood et al., 1992; Colombo et al., 2008). However, the specific mechanisms and systematics involved in Pd mobilization by chloride in weathering environments are currently not well understood and the hypothesized mechanism behind Pd leaching during weathering has not been experimentally investigated.

Adsorption is known to play a key role in controlling the mobility of many metals in the environment (e.g., Brown et al., 1999; Violante et al., 2010). Pd adsorption to iron (oxyhydr)oxides could be an important process involved in retaining this critical element and may explain the frequent association of Pd with these minerals during weathering. Researchers have previously demonstrated that various inorganic Pt, Pd, and rhodium complexes adsorb to many different materials, including shale (Koshcheeva et al., 2016); kaolinite (Takahashi et al., 1999); δ-MnO_2 (Tanaka et al., 2017); and various iron (oxyhydr)oxide phases (Uheida et al., 2006; Kubrakova et al., 2011; Koshcheeva et al., 2016; Tyutyunnik et al., 2016). However, most prior work has not examined the effect of common environmental ligands on adsorption nor the specific mechanisms of binding to mineral surfaces, limiting our understanding of fundamental

processes controlling retention and hindering our ability to predict the behavior of Pd during weathering.

The effect of chloride complexation on Pd adsorption to iron (oxyhydr)oxides under conditions relevant to surface and near-surface weathering of PGE deposits has not been previously investigated. The relative roles of competitive and cooperative processes, such as solution versus ternary surface complexation, are currently unclear. Chloride has been previously found to inhibit the adsorption of other metals like mercury (Kim et al., 2004), cadmium (Benjamin and Leckie, 1982), and silver (Davis and Leckie, 1978), due to the formation of highly stable aqueous chloro-complexes. In contrast, Bargar et al. (1998) found that chloride enhances lead uptake onto goethite through the formation of Pb(II)-chloro ternary surface complexes under acidic conditions. Of most relevance to our work, both Uheida et al. (2006) and Tanaka et al. (2017) found that Pd uptake on Fe_3O_4 nanoparticles and δ-MnO_2, respectively, decreased at higher chloride concentrations. However, these experiments were performed at elevated chloride concentrations (up to 0.5 M) more relevant to marine environments and under pH conditions that were either more acidic or basic than those displayed by terrestrial weathering zones.

In order to determine the role of chloride in enhancing Pd(II) mobility, we investigated adsorption to hematite and 2-line ferrihydrite at pH 4. Pd adsorption isotherms were constructed at a series of chloride concentrations (0.5 to 10 mM) to study the impact of changing Pd speciation on uptake. Hematite was studied because it is a common iron oxide that is frequently observed in relevant weathering zones (e.g., Gray et al., 1996; Traoré et al., 2006; Ndjigui et al., 2008; Ndjigui and Bilong, 2010; Suárez et al., 2010; Aiglsperger et al., 2014; Al-Khirbash and Ahmed, 2021; Ito et al., 2021). Similarly, 2-line ferrihydrite was investigated because it is a

metastable phase that is commonly the first formed iron (oxyhydr)oxide in the environment (Fischer and Schwertmann, 1975; Torrent et al., 1982; Johnston and Lewis, 1983). We modeled Pd speciation in solution to assess the specific impacts of chloride on adsorption. We also assessed the impact of chloride on the surface charge of iron (oxyhydr)oxides using zeta potential measurements. Extended X-ray absorption fine structure (EXAFS) spectroscopy was used to investigate Pd binding mechanisms and possible ternary surface complexation. We developed a surface complexation model of our hematite data to further assess the reaction mechanisms underlying the impact of chloride on Pd binding.

2. MATERIALS AND METHODS

2.1. Mineral Synthesis and Characterization

Hematite was synthesized following a modified version of a previously described forced hydrolysis procedure (Schwertmann and Cornell, 2000). 300 mL of 1 M NaOH was slowly added to 500 mL of a 0.2 M $Fe(NO_3)_3 \cdot 9H_2O$ solution that was continuously stirred, after which 50 mL of 1 M $NaHCO_3$ was also slowly added. The suspension was then aged at 98°C for 5 days. The resulting solids were rinsed with 450 mL ultrapure water (18.2 MΩ cm) using a vacuum filtration setup (0.45 μm MCE filter) to remove excess ions and then resuspended and stored in a constantly stirred aluminum-foil wrapped polypropylene bottle. Multiple batches of hematite were synthesized for use in experiments (see **Table S1**).

Two line ferrihydrite was prepared following an adapted version of a previously described method (Schwertmann and Cornell, 2000). 73.5 mL of 5 M NaOH was slowly added to 125 mL of a 1 M $Fe(NO_3)_3 \cdot 9H_2O$ solution that was continuously stirred. The pH was monitored to ensure that the solution did not exceed pH 8 (to prevent the formation of goethite).

179 The resulting suspension was dialyzed for at least 3 days in ultrapure water, changing the water
180 at least 2 times a day to remove excess ions. The final suspension was stored in an aluminum
181 foil-wrapped polypropylene bottle that was constantly stirred. Each batch of 2-line ferrihydrite
182 was used for experiments within 2 months of synthesis (see **Table S1**) to avoid transformation to
183 more stable phases.

184 A subsample of each mineral suspension was dried solely for mineral characterization.
185 The remaining suspension was used for experimental samples. All hematite batches and the first
186 batch of 2-line ferrihydrite (F1) were dried overnight in a convection oven (70°C for hematite
187 and 40°C for ferrihydrite). A subsample of the second batch of 2-line ferrihydrite (F2) was
188 frozen and freeze-dried. We collected N_2 gas adsorption isotherms with a Quantachrome Nova
189 2000e instrument to determine the Brunauer-Emmett-Teller (BET) specific surface area of each
190 mineral batch (**Table S1**). X-ray diffraction patterns were collected of each mineral batch on a
191 Bruker d8 Advance Diffractometer using Cu Kα radiation to ensure that no other minerals were
192 present (**Fig. S1**). Suspension concentrations were determined gravimetrically. The results of
193 mineral characterization are reported in the Supplementary Material.
194
195 **2.2. Macroscopic Binding Experiments**

196 Palladium adsorption to hematite and 2-line ferrihydrite at up to four different chloride
197 concentrations (0.5, 2, and 10 mM total chloride for both minerals, plus additional data for
198 hematite at 5 mM total chloride) was studied in batch experiments. We chose these
199 concentrations to reflect the chloride concentrations measured in waters interacting with relevant
200 PGE deposits and tailings piles, which can be less than 0.3 mM to greater than 20 mM
201 (McGregor et al., 1998; Alexander et al., 2017; Ahokpossi et al., 2018; Molekoa et al., 2019).

While Pd in natural waters is likely in the tens of pg/kg (sub pM range) and as high as 2 ng/kg (~19 pM) in the vicinity of a PGE deposit (Coker et al., 1991; Cobelo-García et al., 2021), we performed our experiments at higher concentrations of Pd because available analytical techniques cannot quantify dissolved Pd at such low levels when experimentally measuring adsorption isotherms. In order to ensure that the high amounts of Pd used were still soluble, we performed experiments at pH 4, which is within the range of pH values expected in relevant weathering environments where aqueous chloride complexation dominates Pd speciation (Baas Becking et al., 1960; Thompson and Rodgers, 1977; Colombo et al., 2008; Fandeur et al., 2009; Galey et al., 2017; van der Ent et al., 2018; Ito et al., 2021).

A 5 mM $PdCl_2$ stock solution containing approximately 50 mM HCl was prepared from reagent-grade chemicals. A portion of this stock was diluted with ultrapure water to 1 mM Pd for select low chloride experiments (all 0.5 mM chloride experiments; experiment with hematite in 2 mM chloride). In the experiments, solutions of 10 mL total volume containing 0 to 400 μM dissolved Pd were reacted with suspensions of hematite or ferrihydrite at pH 4±0.1 for 24 hours. Experiments with hematite in 2, 5, and 10 mM chloride used a mineral loading of 4 g/L. The experiment with hematite in 0.5 mM chloride was conducted by keeping a constant Pd concentration (10 μM) in all samples and varying the mineral loading from 0.5 to 8 g/L. This distinct approach was used to avoid losses of Pd to sample tube walls and during filtration, which preliminary measurement showed were only substantial when working at much lower initial dissolved Pd concentrations, as would have been required for an experiment using a constant mineral loading. The experiments with hematite in 5 and 10 mM chloride used a batch of hematite with a BET surface area of 24.7 m^2/g; the hematite experiments in 0.5 and 2 mM chloride used a different batch of hematite with a BET surface area of 23.8 m^2/g (**Table S1**). The

225 experiments with 2-line ferrihydrite in 0.5, 2, and 10 mM chloride used mineral loadings of 0.05,
226 1, and 1 g/L (measured BET surface area of 133 m^2/g), respectively, due to the greater amount of
227 adsorption anticipated (**Table S1**). A supplementary experiment was conducted in 10 mM
228 chloride with 1 g/L hematite (BET surface area: 23.9 m^2/g) at pH 3±0.05 to evaluate the pH-
229 dependence of Pd adsorption in chloride-bearing fluids (**Table S1**). Mineral-free blanks and
230 triplicate samples were also prepared. Total chloride in each set of samples was kept constant
231 through the addition of dissolved NaCl stock solutions (10 and 100 mM). All samples were
232 prepared in polypropylene tubes that were wrapped in aluminum foil to inhibit photochemical
233 reactions. After preparation, the samples were continuously mixed using end-over-end rotators.
234 Prior to and after adding the Pd stock solution, as well as at 2 and 21 hours into the
235 experiments, pH was measured and adjusted using HNO_3 and NaOH. For initial experiments
236 (hematite in 2, 5, and 10 mM chloride), the pH was measured with a semi-micro single junction
237 pH electrode filled with a commercial 3.5 M KCl and AgCl solution. However, this was found to
238 add additional chloride to samples via leakage from the porous junction. In order to minimize
239 contamination, the pH in subsequent experiments was measured with a Thermo Scientific™
240 Orion™ semi-micro double junction pH electrode. The outer chamber electrolyte was changed
241 from 3 M KCl to 3 M KNO_3 and the electrode was stored in the same solution during
242 experiments to prevent input of excess chloride in our samples. After 24 hours, the final sample
243 pH was recorded and samples were centrifuged (3901 x g for a minimum of 20 minutes) and
244 filtered using disposable 0.22 μm MCE syringe filters. A portion of the filtrate was immediately
245 acidified to 2% HNO_3 (trace metal grade) for analysis of final aqueous Pd. A separate portion of
246 the filtrate was later diluted with ultrapure water for total chloride determination by ion
247 chromatography using a Thermo Dionex Integrion Ion Chromatograph. We report the chloride

for each set of samples as the average of measured final chloride concentrations in experimental samples ± 1 standard deviation.

The concentration of Pd in samples and blanks was measured by inductively-coupled plasma optical emission spectroscopy (ICP-OES) using a Thermo iCAP 7400 DUO ICP-OES (10 ppm Sc internal standard) or by inductively-coupled plasma mass spectrometry (ICP-MS) using a NexION 2000 PerkinElmer ICP-MS (20 ppb Sc internal standard). Adsorbed Pd was calculated as the difference between starting Pd concentration and measured Pd in solution, normalized to available surface area in each experiment. Mineral-free blanks were used to correct for losses to tube walls and during filtering by assuming a linear relationship between target starting concentration and measured final aqueous Pd in mineral-free blanks to use for calculating initial Pd in mineral-containing samples. Error was calculated by adding in quadrature the sample relative standard deviation from triplicate instrumental measurements, the average error from the weighted calibration curve, and the relative standard deviation from triplicate samples. Any samples for which precipitation was suspected were removed from further data analysis. Single and dual Langmuir adsorption isotherms were fit to each experimental curve using a non-linear least squares method (Levenberg-Marquardt algorithm).

2.3. Thermodynamic Modeling of Pd Speciation

Aqueous Pd speciation for all adsorption experiments was calculated using The Geochemist's Workbench®. We used an altered version of the standard thermodynamic database from the pyGeochemCalc Python package (Awolayo and Tutolo, 2022), which uses the B-dot model for activity coefficients. We updated the formation constants for Pd-OH and -Cl species (**Table S3**) to align with newer values from Rai et al. (2012), including adding $PdCl_3(OH)^{2-}$ and

$Pd(OH)_3^-$ and removing $Pd(OH)^+$. While there is considerable uncertainty and disagreement with regards to the formation constant of $Pd(OH)_{2(aq)}$, which affects predictions of how Pd speciation will change as a function of chloride concentration, we used the lower bound of log K = 5.42 (for the dissociation reaction) suggested by Rai et al. (2012).

The fluid composition of each sample was individually modeled. Speciation was calculated using the measured Pd, chloride, and final pH. Sodium, which was never directly measured, was used as the charge balance. We replotted the adsorption isotherms in terms of the activity of Pd^{2+} to assess the role of aqueous chloride complexation and activity coefficients in driving changes in adsorption.

2.4. Surface Charge

Zeta potential measurements were collected to indirectly assess the effect of chloride uptake on surface charge. Pd-free samples with 0.1 g/L 2-line ferrihydrite or 1 g/L hematite were prepared with 0.5, 2, and 10 mM NaCl at pH 4 ± 0.1 in the same manner as described in **Section 2.2**, although sample sizes were scaled up to 50 mL. Zeta potential was measured with a Malvern ZEN 3600 Zetasizer. A dilution factor of 5 was used for the hematite samples; samples were diluted with pH-adjusted NaCl solutions of the same concentration as the sample. Samples were measured at least in triplicate to account for instrument measurement error.

2.5. EXAFS Spectroscopy

We studied the effect of chloride on Pd binding to iron (oxyhydr)oxides using EXAFS spectroscopy. Samples of Pd adsorbed to hematite and 2-line ferrihydrite were prepared at multiple chloride concentrations (0.5-10 mM) following the same general procedures as the

294 macroscopic binding experiments (**Table S4**). Two samples were prepared with hematite in 10
295 mM total chloride to determine whether the surface species varied as a function of the adsorbed
296 Pd concentration. EXAFS samples were prepared in a similar manner as described in **Section**
297 **2.2**, but sample sizes were scaled up to 50 or 100 mL total volume in order to produce enough
298 solids for analysis. Sample H10h was made with a 30 mM $PdCl_2$ stock solution containing
299 approximately 0.1 M HCl, prepared from reagent-grade chemicals. This sample was also
300 prepared before the discovery that our initial pH electrode setup added excess chloride to
301 samples. All other EXAFS samples were prepared with the 5 mM $PdCl_2$ stock solution and the
302 chloride-free pH electrode setup described in **Section 2.2**. After 24 hours, the solids were
303 collected and packed as a wet paste for analysis using only plastic tools to prevent reduction of
304 Pd by contact with stainless steel or other metals. The solids were packed using two different
305 methods. Hematite samples were centrifuged and the supernatant decanted; the solid was
306 collected and sealed in Delrin sample holders using Kapton tape. For ferrihydrite samples, where
307 the total amount of mineral was too low to permit this approach, the solids were concentrated in
308 solution by centrifuging and decanting a portion of the supernatant and then resuspending the
309 centrifuged solids. A small volume of the concentrated solution was filtered using a reusable
310 syringe with a 0.22 μm MCE membrane. The wet mineral paste collected on the filter membrane
311 was then packed between two layers of Kapton film and sealed with Kapton tape. Prepared
312 samples were immediately stored at -80°C and transported to the beamline in a liquid N_2 dry
313 shipper to prevent them from desiccating or reacting further. The remaining liquid from the
314 supernatant for both sample packing methods was filtered using 0.22 μm MCE syringe filters
315 and analyzed for total dissolved Pd and chloride (**Table 3,S4**) using methods described above.
316 The adsorbed concentrations (**Table 3,S4**) were estimated by measuring aqueous Pd and

317 calculating the theoretical equilibrium adsorbed Pd using the Langmuir isotherms constructed in
318 our macroscopic binding experiments.
319 EXAFS spectra were collected at beamline 4-1 at the Stanford Synchrotron Radiation
320 Lightsource (SSRL), SLAC National Accelerator Laboratory. The incident beam energy was
321 scanned using a cryogenically-cooled Si (220) double-crystal monochromator, with the second
322 crystal detuned by 25% to reduce harmonic contributions. Data were collected in fluorescence-
323 yield using a 32-element solid-state Ge energy-dispersive detector. All data were collected at 77
324 K by cooling in a liquid N_2 cryostat to prevent beam-induced Pd reduction. Preliminary X-ray
325 absorption near-edge structure (XANES) spectroscopy measurements revealed progressive
326 reduction of Pd(II) to metallic Pd when hydrated samples were measured at room temperature.
327 This was observable within 25 minutes of beam exposure. Cryogenic measurements showed no
328 scan-to-scan variation in the XANES spectrum. Data from multiple scans were averaged and
329 corrected for deadtime using the SixPACK interface to IFEFFIT (Newville, 2001; Webb, 2005).
330 Refinement of local structural models to the EXAFS spectra were conducted in SixPACK.
331 Backscattering phase and amplitude functions for fitting were generated in FEFF8L (Ankudinov
332 et al., 1998) with Larch (Newville, 2013) using a modified version of the crystal structure of
333 Pd_2OCl_2 (Dannecker and Thiele, 1986), where two Pd atoms were replaced with Fe. Preliminary
334 structural model fitting of the spectrum of Pd foil obtained an amplitude reduction factor (S_0^2) of
335 0.87, which was then applied for all analyses of samples. The σ^2 value for the Pd-Cl scattering
336 path was set to equal that of the Pd-O scattering path to reduce parameter correlations during
337 fitting. The coordination number of the Pd-Cl path was set to 4 minus the coordination number
338 of the Pd-O path, explicitly assuming a square planar coordination for Pd(II). The FEFF
339 calculation indicated that three multiple scattering paths occurred when Pd was coordinated to O

or Cl. These include Pd-O-O'-Pd, Pd-O-Pd-O'-Pd, and Pd-O-Pd-O-Pd scattering paths or their Cl equivalents (e.g., Pd-Cl-Cl'-Pd), where O'/Cl' indicate an O or Cl backscatter distinct from the initial anion backscatterer in these multiple scattering paths. The coordination numbers for these paths were equal to the coordination number for the corresponding Pd-O or Pd-Cl single scattering. The interatomic distances and σ^2 values were set to be double the values of the corresponding single scattering paths. These constraints required no additional fitting parameters. A single σ^2 value was fit for all second-shell Fe neighbors. A single ΔE_0 was refined for all paths. Spectra were fit in R-space from 1.1 to 4.5 Å using the Fourier transform from a *k*-range of 3 to 13.5 $Å^{-1}$.

2.6. Surface Complexation Modeling

We developed a surface complexation model (SCM), which considers both chemical and electrostatic energetics of reactions at mineral-water interfaces, to evaluate the chemical processes and surface species controlling the impact of chloride on Pd adsorption to hematite. We implemented a diffuse layer model (DLM) (Stumm et al., 1970; Davis et al., 1978; Dzombak and Morel, 1991) in Visual MINTEQ 3.1 (Gustafsson, 2014). The hematite density was set at 2.3 sites/nm^2, a commonly used value for iron oxides (Hwang and Lenhart, 2008; Han et al., 2023). Our model included reactions for the formation of aqueous Pd complexes, surface protonation-deprotonation, and the formation of Pd surface complexes. For aqueous reactions, chloride and hydroxide complexes of Pd were considered using equilibrium constants updated as described in **Section 2.3** (**Table S3**). Equilibrium constants of surface protonation-deprotonation reactions were sourced from Han et al. (2023) (Reactions 1 and 2 in **Table 4**). Electrolyte ion (Na^+ and Cl^-) binding reactions had only a subtle impact on Pd adsorption and were thus not included in the

363 model. The equilibrium constants of reactions sourced from references were adjusted in order to
364 be integrated into this study, which accounted for variations in hematite concentration, surface
365 area, and site density (Sverjensky, 2003, 2006). Detailed procedures for these adjustments can be
366 found in previous work (He et al., 2024). The selection of Pd surface complexation reactions was
367 guided and constrained by our EXAFS results. We simulated adsorption of Pd to hematite under
368 different chloride concentrations. Our modeling approach accounted for multiple combinations
369 of surface complexation reactions with varying stoichiometry. The equilibrium constants for the
370 Pd surface complexation reactions were optimized by minimizing the residual sum of squares
371 between model-generated outputs and experimental data (expressed as μmol/m^2). A forward
372 search for log K values from -30 to 30 in 0.1 increments was performed, followed by fine-tuning
373 with 0.01 increments.

374

375 **3. RESULTS**

376 **3.1. Effect of Chloride on Macroscopic Pd(II) Binding**

377 Progressively increasing dissolved chloride concentrations from 0.5 to 10 mM suppresses
378 Pd(II) adsorption to both hematite and 2-line ferrihydrite (**Fig. 1**). For the same final aqueous Pd
379 concentration, greater adsorption is consistently observed under lower chloride concentration
380 across the full range of final dissolved Pd concentrations. The obtained surface area-normalized
381 Pd coverages calculated were substantially greater for ferrihydrite than for hematite (**Fig. 1**).
382 However, the surface area of ferrihydrite obtained from BET (133 m^2/g) was likely an
383 underestimate caused by particle aggregation during drying, which decreases the measurable
384 surface area (Schwertmann and Cornell, 2000). In contrast, the theoretical surface area of 2-line
385 ferrihydrite nanoparticles, assuming a perfectly spherical particle shape, is approximately 600

386 m^2/g (Schwertmann and Cornell, 2000). The reported Pd coverages (**Fig. 1b**) are thus likely
387 substantially overestimated by a factor of 4 to 5 and would be similar to those obtained for
388 hematite if the true ferrihydrite surface area is similar to the idealized value.

389 We found that for all experiments, the adsorption data were generally reproduced well
390 with an unweighted single Langmuir isotherm (**Fig. 1**). Initial fits to the 0.5 and 2 mM total
391 chloride experiments for hematite obtained substantially lower surface-area normalized
392 absorption capacities than for higher chloride concentrations. However, the binding capacities in
393 those experiments were poorly constrained by the data because Pd solubility limits prevented
394 extending the measurements to conditions that produce an adsorption plateau. For the
395 experiments with ferrihydrite as well as with hematite at higher chloride concentrations, we
396 observed no systematic shift in the binding capacity as a function of chloride concentration
397 (**Table 1**). In addition, there is no clear mechanism through which the adsorption capacity of
398 hematite would substantially decrease when total dissolved chloride concentration changed from
399 5 mM to 2 or 0.5 mM. The reported Langmuir isotherm fits (**Table 1**) thus employed a fixed
400 binding capacity for the two lower-chloride hematite experiments, using the same value as the
401 other hematite experiments at pH 4 (1.3 $\mu mol/m^2$).

402 For both ferrihydrite and hematite, the decreasing favorability of adsorption with
403 increasing chloride is reflected in the smaller apparent affinity constant (K) from the Langmuir
404 isotherm fits (**Table 1**). Additionally, despite the apparent differences in binding capacity
405 between minerals, the affinity constants of the Langmuir fits for the ferrihydrite data are similar
406 to values for the hematite data at the same chloride concentrations (**Table 1**), indicating that Pd
407 has a similar adsorption affinity for hematite and 2-line ferrihydrite at all chloride concentrations.
408 When the adsorption data are normalized to the calculated maximum binding capacities,

409 hematite and ferrihydrite data at the same chloride concentrations nearly overplot (**Fig. 2**). This
410 indicates that the two minerals display similar binding affinities but different binding capacities
411 (resulting from different surface site abundances on a per-mass basis), which is reflected in the
412 obtained Langmuir isotherm parameters (**Table 1**).

413

414 **3.2. Aqueous Complexation and Surface Charge Effects on Pd Adsorption**

415 The observed suppression of Pd adsorption to iron (oxyhydr)oxides by aqueous chloride
416 has multiple potential mechanisms, including changes in aqueous speciation, activity
417 coefficients, surface charge, and surface speciation. We used aqueous speciation calculations and
418 measurement of surface charging phenomena to assess potential thermodynamics effects on
419 adsorption. Assuming equilibrium controls, all adsorption reactions will respond to changes in
420 the activity of the Pd^{2+} aqua ion. Increasing total dissolved chloride concentration from 0.5 mM
421 to 10 mM across our primary experiments at pH 4 substantially shifts Pd aqueous speciation
422 from being dominated by $Pd(OH)_{2(aq)}$ to a series of Pd-chloro complexes (**Fig. 3a**). At all
423 chloride concentrations investigated, Pd^{2+} is predicted to be a minor species (**Fig. 3b**). When
424 replotted in terms of the activity of Pd^{2+} rather than total dissolved Pd, adsorption isotherms for
425 hematite and ferrihydrite shift to more similar values but do not overplot, especially at higher
426 total chloride (**Fig. 4**). This suggests that shifts in aqueous speciation are partially responsible for
427 the effect of chloride but do not fully explain the observed behavior. These calculations account
428 for changes in activity coefficients for dissolved species, which for Pd^{2+} is 0.89 at in 0.5 mM
429 NaCl and 0.66 in 10 mM NaCl, a decrease of 26%. The other species present are lower-charge or
430 neutral, and thus have smaller or no change in their activity coefficients. This shows that activity

corrections for solution species have negligible effects on Pd adsorption behavior under the conditions studied.

The inability to fully account for shifts in adsorption behavior via aqueous speciation and activity corrections suggests that additional effects are at play, such as the formation of Pd-Cl ternary surface complexes or changes in surface charge. That the isotherm behavior appears to invert when replotted as a function of $a_{Pd^{2+}}$ (adsorption appears more favorable for the higher chloride concentrations) suggests ternary surface complexes may form. For hematite, the 0.5 mM and 2 mM chloride isotherms appear to overlap when replotted in this way, but this effect is not observed for the ferrihydrite isotherms (**Fig. 4**). At higher total chloride, the isotherms clearly do not overlap (**Fig. 4**), indicating that variations in aqueous chloride complexation cannot explain the differences in adsorption observed. We acknowledge that this assessment relies on the accuracy of the thermodynamic data for aqueous Pd speciation, and errors in such data would thus shift this assessment.

In order to assess the relative role of surface charge effects due to chloride adsorption, zeta potential was measured for Pd-free samples containing varying amounts of NaCl. At all chloride concentrations, the measured zeta potential for all minerals was positive (**Table 2**), indicating a positive surface charge. The measured zeta potential values at all chloride concentrations for ferrihydrite were within 1 standard deviation (**Table 2**). While there was more variation in the measured zeta potential with changing chloride concentration for hematite, the measured zeta potentials were all still within 2 standard deviations (**Table 2**). This similarity suggests that surface charge for each mineral was likely constant despite changing chloride concentrations. This is consistent with negligible chloride adsorption to hematite and ferrihydrite at pH 4. In all but one experiment, the difference in average chloride concentrations between our

454 mineral-free controls and experimental samples is within one standard deviation, although in
455 some experiments this may also be affected by contamination effects from our initial pH
456 electrode setup. Note that we do not report numerical values for the amount of adsorbed chloride
457 because this could not be quantified.
458
459 **3.3. Surface Binding Mechanisms**
460 We assessed the impact of chloride on Pd binding mechanisms using EXAFS
461 spectroscopy because correction for changes in aqueous speciation cannot explain the variability
462 in the adsorption behavior alone, implying that ternary surface complexation occurs. The set of
463 EXAFS spectra for Pd adsorbed to hematite and ferrihydrite under varying chloride
464 concentrations and Pd surface coverages display isosbestic points (**Fig. 5**) which suggests two-
465 component mixing. Notably, oscillations in the EXAFS spectra weaken/flatten between k = 9 to
466 12 $Å^{-1}$ at low chloride concentration (**Fig. 6a**). For all samples, the Fourier transform magnitudes
467 of the spectra have two overlapping features at approximately 1.5 and 1.8 Å (**Fig. 6b**), which are
468 consistent with those previously obtained for O and Cl neighbors at ~2.0 and ~2.3 Å,
469 respectively (Bazarkina et al., 2014; Tanaka et al., 2017). This suggests that the primary spectral
470 variations are caused by changes in the coordination number of O and Cl neighbors. Principal
471 component analysis (PCA) indicates that 98.8% of the variance in the spectra are describes by
472 two components, and the indicator (IND) parameter minimizes at two components (**Table S5**).
473 All spectra are generally reproduced well with two components, although reproduction of spectra
474 from low chloride conditions are improved by the addition of a third component (**Fig. S4**). The
475 improvement from adding the third component may reflect slight variations in coordination

environmental on hematite versus ferrihydrite or shifts in weak second shell features that do not fully correlate with changes in O and Cl neighbors.

A FEFF-based structural model was developed to evaluate the systematic variations in the coordination and binding configuration of Pd on hematite and ferrihydrite surfaces. The first coordination shell was modeled as a mixture of oxygen neighbors at ~2.0 Å and chlorine neighbors at ~2.3 Å. The total coordination number of this shell was fixed to 4, reflecting the square planar nature of Pd(II). The mean-square displacement (σ^2) was set to be identical for the O and Cl neighbors because the overlap of the spectral features from these backscatterers introduces substantial correlations that prevent distinct values from being refined. Second-shell features between ~3.2 and ~4.0 Å (R+ΔR) in the Fourier transform spectra (**Fig. 6b,c**) appear to vary systematically with the intensity of the feature from Cl neighbors appearing at ~1.8 Å (R+ΔR), suggesting a possible origin from multiple-scattering. Analysis of the FEFF calculation for Pd_2OCl_2, in which Pd is coordinated to two O and two Cl neighbors, reveals a set of three linear multiple scattering pathways of identical path length for each atom type, consisting of Pd-X-Pd-X'-Pd, Pd-X-Pd-X-Pd, and Pd-X-X'-Pd, where X = O or Cl and the prime indicates a distinct O or Cl neighbor. All three multiple scattering paths for both O and Cl were added to the model, with the coordination number (N) equal to N for the first-shell single scattering path for that atom type and both the interatomic distance (R) and σ^2 set to double their values for the corresponding first-shell paths. This multiple scattering reproduced Fourier transform features at 3.6 to 4.0 Å (R+ΔR) but not at shorter distances.

Reproducing the Fourier transform features at intermediate distances required the addition of three separate Pd-Fe paths with interatomic distance of ~2.95 Å, ~3.15 Å, and ~3.65 Å. The first two distances require that Pd occupies an edge-sharing bidentate coordination to an

499 iron octahedron, with the two distances possibly reflecting different Fe-O bond lengths (many
500 iron (oxyhydr)oxides have distorted octahedra with Fe-O bonds of ~1.95 and ~2.10 Å), different
501 angular geometries of bidentate Pd relative to the edge of an iron octahedron, or shifts in bond
502 angles for complexes with and without distal Cl ligands (**Fig. S3a,b**). The longer Pd-Fe distance
503 is consistent with Pd in either a monodentate or corner-sharing bidentate configuration, the latter
504 bridging between two octahedra (**Fig. S3c,d**). Preliminary fitting revealed the presence of this
505 longer Pd-Fe shell in spectra where the coordination number of Cl was >2. If a species occurs
506 with 3 Cl ligands, then this longer Pd-Fe path must correspond to a monodentate complex since
507 Pd could only form one Pd-O bond. The complex corresponding to each of the three Pd-Fe
508 distances should thus each have 1 Fe neighbor. Assuming these neighbors represent all Pd
509 species, their N values for these three Pd-Fe paths must sum to 1 and their individual values
510 correspond to the fractional coverage of each complex type. We thus constrained the N values
511 for these paths to equal 1 in our model. To decrease parameter correlations, the model also fit a
512 single σ^2 value for the three Pd-Fe paths.

513 Our structural model fits reproduce the data well (**Fig. 6**) and yields between 1.3 and 2.6
514 Cl neighbors and between 1.4 and 2.7 O neighbors (**Table 3**). While the Pd-O and Pd-Cl
515 interatomic distances are essentially identical in all samples (the variations of ~0.02 Å are within
516 the expected accuracy of EXAFS spectroscopy), the adsorbed Pd becomes coordinated to a
517 greater number of Cl atoms with increasing aqueous chloride. This trend is observed for both 2-
518 line ferrihydrite and hematite, although the Pd adsorbed to ferrihydrite is coordinated to fewer Cl
519 atoms compared to hematite at the same aqueous chloride concentration.

520 The observed range of coordination numbers for Cl (1.3 to 2.6) requires that at least two
521 species are present, one having 1 or fewer Cl ligands and a second having 3 or more such

522 ligands. However, the invariance of Pd-O and Pd-Cl bond length as well as their σ^2 values with
523 the number of O and Cl neighbors precludes unambiguous determinations of the number of
524 surface species. For example, a mixture of three surface species contain 1, 2, and 3 Cl neighbors,
525 each having similar Pd-O and Pd-Cl bonds properties, would produce the same isosbestic points
526 (**Fig. 5)** and PCA results (**Table S5, Fig. S4**) as observed here. Surface species with 0 or 4 Cl
527 ligands are not needed to explain the data but we cannot exclude their occurrence. Evaluating
528 their occurrence may be technically challenging because of the low solubility of Pd in the
529 absence of a complexing ligand like chloride and the anticipated low amount of adsorption at the
530 very high Cl concentrations required to possibly form a $PdCl_4$ surface species. The EXAFS
531 results thus suggest that there are two to three Pd surface species forming on hematite and
532 ferrihydrite as dissolved chloride concentration varies.
533 The addition of three Fe neighbors to the model resulted in generally consistent
534 interatomic distances. The three Pd-Fe distances varied little among the samples, averaging
535 2.93±0.01, 3.11±0.02, and 3.64±0.03 Å (**Table 3**), indicating consistent coordination geometries
536 on both minerals under varying chloride concentration. This agrees with the PCA results (**Table**
537 **S5, Fig. S4**) finding limited variation among the spectra. The σ^2 values (0.002 to 0.005) indicate
538 low disorder in the Pd-Fe coordination, consistent with the distance indicating inner-sphere
539 binding. The two shorter Pd-Fe interatomic distances, associated with bidentate edge-sharing
540 complexes, do not show clear trends with dissolved chloride concentration or the number of Cl
541 neighbors, but trends may be masked by the large relative uncertainty in the coordination
542 numbers. The longest Pd-Fe path around 3.64 Å is likely associated with monodentate bonding
543 because the coordination number of Cl is often >2, requiring some complexes with three Cl
544 neighbors. Since Pd can only form four bonds in square planar coordination, a species bound to

three chlorines may only form one bond to a surface oxygen. The two shorter Pd-Fe paths can only be explained by an edge-sharing bidentate geometry, and so the longer distance must correspond to a monodentate species. The fractional abundance of this species may weakly correlate with the number of Cl neighbors ($R^2 = 0.56$), although this correlation is primarily induced by the ferrihydrite sample in 0.5 mM dissolved chloride (F0.5h), with no clear trend among the other samples ($R^2 = 0.12$ with F0.5h removed; **Fig. S5**).

3.4. Surface Complexation Modeling

A surface complexation model (SCM) was developed to explore the impact of chloride on Pd surface speciation within a thermodynamic framework. Only the hematite data were modeled because of uncertainty in the surface area of ferrihydrite (**Section 3.1**) and the similar adsorption behavior displayed by the two minerals (**Fig. 2**). Adsorption was modeled by including three inner-sphere hematite-Pd-Cl ternary surface complexes with varying numbers of Cl ligands: $(>FeO)_2PdCl^-$, $(>FeOH_2)(>FeOH)PdCl_2^+$, and $>FeOHPdCl_3^-$ (Reactions 3-5 in **Table 4**). The SCM captures the variation in Pd adsorption as a function of dissolved chloride concentration (**Fig. 7**). Adsorption is suppressed with increasing chloride because of decreased Pd^{2+} activity (**Fig. 3b**). However, higher chloride concentrations also promote the formation of hematite-Pd-Cl ternary complexes with a higher number of Cl ligands (**Fig. S6**). At low chloride concentrations (0.5 mM), the dominant adsorbed Pd species is predicted to be $(>FeO)_2PdCl^-$ (**Fig. S6d**). As chloride concentrations increase beyond 2 mM, the surface species with two Cl atoms, $(>FeOH_2)(>FeOH)PdCl_2^+$, becomes dominant (**Fig. S6**). Our EXAFS fit results (**Table 3**) indicated that a surface complex with at least 3 Cl atoms is present at high chloride concentrations. We thus included a surface species containing three Cl atoms, $>FeOHPdCl_3^-$

(**Fig. S6**). This third complex must be a monodentate species because Pd is square planar and thus can only make one bond to a surface oxygen group when bound to three chlorides.

The predictive capability of the developed SCM was evaluated by simulating Pd adsorption at pH 3 in 10 mM chloride in comparison to measurements made under the same conditions (**Fig. S7**). This additional dataset was collected for SCM testing (see **Supplementary Material**) and was not used in the optimization of the log K values. Our model successfully predicts the observed decrease in adsorption at pH 3 compared to pH 4 (**Fig. S7**). The predicted decrease in the concentration of all modeled adsorbed Pd species results from the greater protonation of surface groups. The dominant aqueous species change little from what is observed at pH 4 (**Fig. 3**) because these are primarily Pd-Cl complexes in 10 mM chloride. The $Pd(OH)_{2(aq)}$ complex decreases in concentration by 2 orders of magnitude but it only comprises 0.2% of aqueous species at pH 4, so this change has an overall negligible effect on aqueous speciation. At pH 3 in 10 mM chloride, the predicted dominant adsorbed Pd species is $(>FeOH_2)(>FeOH)PdCl_2^+$, with $>FeOHPdCl_3^-$ responsible for ~25% of Pd binding (**Fig. S7b**).

4. DISCUSSION

4.1. Impacts of Chloride on Macroscopic Pd Adsorption Behavior

The experimental results in this study (**Fig. 1**) consistently show that dissolved chloride concentration strongly controls the adsorption behavior of Pd on the iron (oxyhydr)oxides hematite and ferrihydrite under weakly acidic conditions. This effect is qualitatively consistent with the strong complexation of Pd with chloride in solution (Rai et al., 2012). However, quantitative prediction of the suppression of Pd adsorption by chloride based solely on aqueous complexation behavior would have substantially overestimated this effect. Renormalization of

591 measured adsorption isotherms to the activity of free Pd^{2+} (**Fig. 4**), EXAFS spectroscopy (**Fig.**
592 **6**), and surface complexation modeling (**Fig. 7,S4**) all demonstrate that Pd adsorption involves
593 the formation of Pd-Cl surface species. Their formation partially offsets the solubilizing effects
594 of dissolved chloride, and failure to account for these species would lead to overprediction of
595 aqueous Pd concentrations (and underprediction of adsorption).

596 An additional challenge in predicting how chloride impacts Pd adsorption in the absence
597 of the new findings of this study are the lack of agreement regarding the favorability of
598 hydroxide and chloride complexes of palladium in solution. While there has been general
599 consensus regarding the formation constants for $PdCl_n^{2-n}$ complexes (Tait et al., 1991; Boily and
600 Seward, 2005), uncertainties in the solubility of palladium hydroxide solids and stability of Pd
601 hydrolysis and hydroxy-chloro species in solution raise substantial challenges to accurate
602 prediction (Byrne and Kump, 1993; Van Middlesworth and Wood, 1999; Boily et al., 2007;
603 Koroleva et al., 2012; Rai et al., 2012). For modeling conditions in terrestrial weathering
604 environments, the largest challenge is posed by the relative balance of hydrolysis versus chloride
605 complexation. Specifically, continued uncertainty in the stability constant of the $Pd(OH)_{2(aq)}$
606 species (Rai et al., 2012) affects the predictions of Pd aqueous speciation. The SCM results in
607 this study are dependent on the specific formation constants used for aqueous complexation
608 (**Table S3**). Any future revisions to the hydrolysis constants for Pd will require re-optimization
609 of the SCM to the experimental data, which are independent of aqueous thermodynamic data.
610 Accurate prediction of the effects of chloride on Pd adsorption at higher pH based on the present
611 data would require greater certainty in the stability of the second hydrolysis product of Pd.

612 The results of this study also demonstrate that the binding affinity for Pd varies little
613 between highly crystalline (hematite) and nanoparticulate (ferrihydrite) minerals. The primary

differences in the reactivity of these phases towards Pd are their surface site densities on a per-mass basis. Phase transformation of ferrihydrite to hematite, such as during progressive stages of weathering (Cornell and Schwertmann, 2003), would only alter the retention of Pd through a decrease in the number of surface sites associated with particle size coarsening. In such systems, iron (oxyhydr)oxide particle size, not mineralogy, would be the major solid-phase control on the retention of Pd. However, the coarsening associated with iron (oxyhydr)oxide mineralogical transformation may not appreciably affect net Pd retention because of the high solid:water ratio of weathering environments as well as the low total dissolved Pd concentrations. Under such conditions, a very high mass fraction of the total Pd in the system (>99.9%) would be adsorbed and surface sites would be far from saturated, so the loss of surface sites from particle size coarsening would increase dissolved Pd but negligibly impact the total amount of adsorbed Pd.

4.2. Mechanisms Controlling Pd Adsorption in Chloride-Bearing Fluids

The spectroscopic analysis in this study demonstrates that Pd-Cl ternary complexes dominate Pd surface species on iron (oxyhydr)oxide surface under the conditions studied (**Table 3**). No experimental conditions provided evidence for a binary (i.e., Cl-free) Pd surface complex, and only ternary complexes were required to construct a SCM that reproduces the macroscopic Pd adsorption data (**Fig. 7**). A dominant feature of Pd surface speciation observed by EXAFS and reproduced by the SCM is that the average number of Cl ligands per Pd on hematite increases with increasing dissolved chloride concentration. For ferrihydrite, the number of Cl neighbors observed in the EXAFS spectra was systematically lower than for hematite at similar dissolved chloride concentrations (**Table 3**). This may have resulted from the slightly lower chloride concentrations inadvertently used when preparing the ferrihydrite EXAFS samples

637 (**Table 3**), e.g., 9.7 – 10 mM chloride for hematite versus 8.9 mM chloride for ferrihydrite.
638 However, the macroscopic adsorption data for ferrihydrite are shifted slightly compared to
639 hematite under statistically identical chloride concentrations (**Fig. 2**). This indicate a slight
640 difference in binding affinity, which would be consistent with subtle difference in surface
641 speciation between the two minerals.

642 There is generally good agreement between the EXAFS spectral fits and the SCM. The
643 EXAFS spectra clearly require a Pd surface species with at most 1 Cl ligand and another with at
644 least 3 Cl ligands to reproduce the range of coordination numbers for Cl obtained during fitting.
645 Similarly, the SCM utilizes a mixture of mono-, di-, and trichloro Pd ternary surface complexes
646 (**Fig. S6**). In addition, the weak variation in the number of Cl neighbors with surface coverage at
647 10 mM dissolved Cl seem by EXAFS (**Table 3**) is in general agreement with the SCM, where
648 the relative proportion of mono-, di-, and trichloro species varies by <5% between these two
649 conditions (**Fig. S6a**).

650 However, while the EXAFS spectra and SCM have identical trends, there are some
651 quantitative differences. EXAFS consistently observes a greater number of Cl neighbors, and
652 thus a greater percentage of di- and trichloro Pd surface species on hematite, than the SCM under
653 most conditions. For example, EXAFS identifies 1.9 Cl neighbors for Pd adsorbed in 0.5 mM
654 chloride and 2.5-2.6 Cl neighbors (samples H10l and H10h, **Table 3**) in approximately 10 mM
655 chloride, whereas the SCM predicts the average number of Cl ligands to be 1.05 and 2.07-2.13
656 under the same conditions.

657 This discrepancy between spectroscopy and surface complexation modeling has multiple
658 potential origins. Constraining the σ^2 values for the O and Cl shells to be identical during the
659 fitting of the EXAFS spectra would overestimate the number of Cl neighbors if σ^2 for the Cl

660 shell is actually smaller than for the O shell. Errors in the stability constants of aqueous species
661 (discussed in **Section 4.1**) would systematically shift the surface speciation predicted by the
662 SCM. Likewise, it is possible that a different set of ternary complexes, such as with different
663 protonation states, could also reproduce the data but differ slightly in the distribution of species
664 with 1, 2, and 3 Cl ligands. Finally, the freezing process during EXAFS sample preparation
665 could have increased dissolved chloride concentrations before complete freezing occurred,
666 shifting to a slightly greater number of Cl neighbors. Notably, EXAFS analysis of the
667 ferrihydrite samples reveal a systematically lower number of Cl neighbors than for hematite
668 under the same chloride concentrations (**Table 3**), and in much better agreement with the SCM.
669 The ferrihydrite samples were thinner and likely froze more rapidly because of their different
670 preparation for EXAFS measurement, potentially decreasing artifacts associated with the
671 freezing process. Irrespective of these quantitative differences, the EXAFS results and SCM are
672 in overall good agreement and consistently demonstrate that Pd adsorbs solely as chloro ternary
673 surface complexes, with no evidence for a binary (i.e., Cl-free) surface species.
674 While no prior studies have investigated the mechanisms of Pd adsorption to iron
675 (oxyhydr)oxides, with or without chloride, investigation of Pd adsorbed to δ-MnO_2 (Tanaka et
676 al., 2017) provides a point of comparison. Both our study and this prior work identified bidentate
677 edge-sharing complexes, with Pd-Fe/Mn distance around 2.95 Å. This observation suggests that
678 edge-sharing is a common inner-sphere binding mode for Pd. Tanaka et al. (2017) also observed
679 longer Pd-Mn interatomic distances at ~3.5 Å, which they interpreted as bridging bidentate
680 complexes. Our study observes even longer Pd-Fe distance of ~3.64 Å. This difference may
681 reflect the larger size of Fe(III) octahedra compared to Mn(IV) octahedra. However, the clear
682 occurrence of trichloride Pd complexes on iron (oxyhydr)oxides requires that this distance

683 originate from a monodentate complex, so the greater length may also reflect differences in
684 coordination to the surface. Surprisingly, the Pd surface complexes on δ-MnO_2 lack any Cl
685 neighbors, being fully coordinated to O, despite having been prepared in 0.1 M and 0.5 M NaCl
686 (i.e., 10 to 50 times the maximum chloride concentration in the present study). The higher pH of
687 those studies and negative surface charge of δ-MnO_2 may inhibit formation of negatively-
688 charged Pd-Cl surface complexes (Tanaka et al., 2017). This lack of ternary complexation may
689 also explain the difference in the longer Pd-Mn/Fe distances between hematite and δ-MnO_2.
690 Further, the presence of two Pd-Fe distances (~2.93 Å and 3.11 Å) associated with bidentate
691 edge-sharing complexes on hematite may result from different numbers for Cl ligands on each
692 complex, an effect that would not occur on δ-MnO_2 if it inhibits chloride ternary complexes from
693 forming.
694
695 **4.3. Conditions Promoting Greater Mobility of Pd in Weathering Zones**
696 In their study of Pd and Pt behavior in soils above the Stillwater Complex, Fuchs and
697 Rose (1974) proposed that chloride complexation was likely responsible for the depletion of Pd
698 relative to Pt. Studies of other weathering zones have found a similar depletion of Pd relative to
699 Pt (Evans et al., 1994; Oberthür et al., 2003; Oberthür and Melcher, 2005; Traoré et al., 2006;
700 Ndjigui et al., 2008; Locmelis et al., 2010; Suárez et al., 2010; Ito et al., 2021). However, even if
701 Pd is solubilized, adsorption could limit the mobility of this metal; the effect of chloride
702 complexation on adsorption in conditions relevant to these terrestrial environments had not been
703 previously investigated. Our experiments have shown that chloride, in addition to solubilizing
704 Pd, also inhibits Pd adsorption to two environmentally relevant iron (oxyhydr)oxides.
705 Observations of Pd enrichment in the iron (oxyhydr)oxide-rich zones of laterites (e.g., Gray et

al., 1996; Ndjigui et al., 2008; Ndjigui and Bilong, 2010; Al-Khirbash and Ahmed, 2021; Ito et al., 2021) may be the result of Pd retention through adsorption processes. Adsorption is also a key intermediate step during coprecipitation, and conditions that affect Pd adsorption to iron (oxyhydr)oxides will also thus impact its incorporation into the structure of weathering products.

While Fuchs and Rose (1974) suggested a concentration of 10 ppm (~0.28 mM) chloride was a reasonable assumption for soil water in the Stillwater Complex, the relevant concentrations of chloride in these environments may be substantially greater. Platinum-group element deposits frequently contain elevated levels of halogens, thought to be a fingerprint of PGE mineralization processes (e.g., Ballhaus and Stumpfl, 1986; Boudreau et al., 1986; Willmore et al., 2000; Boudreau, 2016; Parker et al., 2022). These anomalies are likely responsible for the high concentrations of chloride measured in tailings pore water (McGregor et al., 1998) and in groundwater interacting with a PGE deposit (Alexander et al., 2017; Ahokpossi et al., 2018; Molekoa et al., 2019), which are much greater than the estimate of Fuchs and Rose (1974). At the more elevated chloride concentrations associated with many PGE deposits, Pd will be partially mobilized as Pd-Cl aqueous complexes when the pH is below 5 to 6 (Colombo et al., 2008; Rai et al., 2012). The fraction retained via adsorption to iron(oxyhydr)oxides will be controlled by the dissolved chloride concentration as well as the abundances and surface areas of mineral sorbents.

In laterites that develop above ultramafic rocks (representative of the oxidized zones above PGE deposits), researchers have measured zones with low pH (3.5-5.5), which is also where iron (oxyhydr)oxides are most abundant (Thompson and Rodgers, 1977; Mann, 1984; Fandeur et al., 2009; Ndjigui and Bilong, 2010; Galey et al., 2017; van der Ent et al., 2018; Ito et al., 2021). Additionally, local microenvironments around weathering sulfide grains may be much

729 more acidic than the bulk system pH (e.g., Dockrey et al., 2014). Our experiments, conducted at
730 pH 4, demonstrate that chloride is a major control on the retention of Pd in these weakly acidic
731 weathering zones.

732 We also observed a lower apparent adsorption affinity for hematite at pH 3 (**Fig. S2**,
733 **Table S2**), a trend that is captured by our SCM (**Fig. S7**). This observation suggests that Pd will
734 be mobilized to a greater extent in more acidic environments. However, as discussed in **Section**
735 **4.1**, predicting the effect of pH on Pd adsorption, particularly an increase in pH, with our SCM is
736 challenging, given uncertainties in the formation constants for Pd species. Additionally, as pH
737 increases, other ligands, particularly ammonia and organic compounds such as oxalate and
738 acetate, are predicted to be more important for Pd speciation (Wood et al., 1989; Wood et al.,
739 1994; Colombo et al., 2008); chloride complexation is unlikely to play a substantial role in
740 mobilizing Pd and controlling speciation in these weathering zones under more neutral to basic
741 conditions. When Pd migrates from these weakly acidic, near-surface weathering zones to zones
742 of higher pH at depth, other ligands may begin to dominate Pd speciation or the lower solubility
743 of Pd under neutral conditions could lead to precipitation.
744
745 **5. CONCLUSION**
746 Chloride, a common ligand in waters during the weathering of PGE deposits, impacts Pd
747 adsorption to two environmentally relevant iron (oxyhydr)oxides via two distinct mechanisms.
748 Aqueous chloride complexation suppresses adsorption at high chloride concentrations. However,
749 this effect is partially counteracted by the formation of Pd-Cl ternary surface complexes that
750 enhance adsorption at high chloride concentrations. While we overall observe a net inhibition of
751 Pd adsorption as chloride concentration increases, predicting Pd behavior accurately requires

accounting for these two competing mechanisms that control Pd adsorption. In the weakly acidic, chloride-rich weathering zones that develop above PGE deposits, Pd will be transported as a chloride complex. Chloride is thus a key control on Pd retention by iron (oxyhydr)oxides in weakly acidic, near-surface weathering environments.

ACKNOWLEDGEMENTS

This project was supported by the U.S. Department of Energy (DOE), Office of Science, Office of Basic Energy Sciences, Critical Minerals and Materials program under Award Number DE-SC0022213. E.G.W. acknowledges support by a National Science Foundation Graduate Research Fellowship under Grant No. 2139839. Any opinions, findings, and conclusions or recommendations expressed in this material are those of the author and do not necessarily reflect the views of the National Science Foundation. Use of the Stanford Synchrotron Radiation Lightsource, SLAC National Accelerator Laboratory, is supported by the DOE, Office of Science, Office of Basic Energy Sciences under Contract No. DE-AC02-76SF00515. The authors thank beamline scientists Erik Nelson and Ryan Davis for their assistance with data collection at SSRL. ICP-MS, BET, and zeta potential analyses were performed at the Chemical and Environmental Analysis Facility at Washington University in St. Louis. The authors thank Sanmathi Chavalmane, Greg Ledingham, Olwen Stagg, Yihang Fang, Ivey Wang, and Elmira Ramazanova for assistance with analytical instruments and data collection.

CRediT Author Statement

Emily G. Wright: Conceptualization, Methodology, Formal Analysis, Investigation, Data Curation, Writing – original draft, Writing – review & editing, Validation, Visualization.

Xicheng He: Methodology, Software, Formal Analysis, Writing – original draft, Writing – review & editing. **Elaine D. Flynn:** Methodology, Investigation, Writing – review & editing. **Daniel E. Giammar:** Methodology, Resources, Software, Formal Analysis, Writing – review & editing, Funding acquisition. **Jeffrey G. Catalano:** Conceptualization, Software, Resources, Methodology, Formal Analysis, Writing – original draft, Writing – review & editing, Supervision, Project administration, Funding acquisition.

Data Availability

Data are available through Mendeley Data at https://doi.org/10.17632/45dzm7mgsp.1.

Appendix A. Supplementary Material

The Supplementary Material contains additional information about mineral batches used in experiments and sample preparation for EXAFS spectroscopy. Results from an experiment conducted at pH 3 are presented. We also provide additional details about Pd surface speciation in our surface complexation model.

References

Ahokpossi D. P., Atangana A. and Vermeulen P. D. (2018) Hydro-geochemical characterizations of a platinum group element groundwater system in Africa. *J. Afr. Earth Sci.* **138**, 348-366.

Aiglsperger T., Proenza J. A., Zaccarini F., Lewis J. F., Garuti G., Labrador M. and Longo F. (2014) Platinum group minerals (PGM) in the Falcondo Ni-laterite deposit, Loma Caribe peridotite (Dominican Republic). *Miner. Deposita* **50**, 105-123.

Al-Khirbash S. A. and Ahmed A. H. (2021) Distribution and Mobility of Platinum-Group Elements in the Late Cretaceous Ni-Laterite in the Northern Oman Mountains. *J. Geophys. Res. Solid Earth* **126**, e2021JB022363.

Alexander A., Ndambuki J., Salim R. and Manda A. (2017) Assessment of Spatial Variation of Groundwater Quality in a Mining Basin. *Sustainability* **9**, 823.

Ankudinov A. L., Ravel B., Rehr J. J. and Conradson S. D. (1998) Real-space multiple-scattering calculation and interpretation of x-ray-absorption near-edge structure. *Phys. Rev. B* **58**, 7565-7576.

Awolayo A. N. and Tutolo B. M. (2022) PyGeochemCalc: A Python package for geochemical thermodynamic calculations from ambient to deep Earth conditions. *Chem. Geol.* **606**, 120984.

Baas Becking L. G. M., Kaplan I. R. and Moore D. (1960) Limits of the Natural Environment in Terms of pH and Oxidation-Reduction Potentials. *J. Geol.* **68**, 243-284.

Ballhaus C. G. and Stumpfl E. F. (1986) Sulfide and platinum mineralization in the Merensky Reef: evidence from hydrous silicates and fluid inclusions. *Contr. Mineral. and Petrol.* **94**, 193-204.

Bargar J. R., Brown G. E. and Parks G. A. (1998) Surface complexation of Pb(II) at oxide-water interfaces: III. XAFS determination of Pb(II) and Pb(II)-chloro adsorption complexes on goethite and alumina. *Geochim. Cosmochim. Acta* **62**, 193-207.

Bazarkina E. F., Pokrovski G. S. and Hazemann J.-L. (2014) Structure, stability and geochemical role of palladium chloride complexes in hydrothermal fluids. *Geochim. Cosmochim. Acta* **146**, 107-131.

Becker M., Wiese J. and Ramonotsi M. (2014) Investigation into the mineralogy and flotation performance of oxidised PGM ore. *Miner. Eng.* **65**, 24-32.

Benjamin M. M. and Leckie J. O. (1982) Effects of Complexation by Cl, SO_4, and S_2O_3 on Adsorption Behavior of Cd on Oxide Surfaces. *Environ. Sci. Technol.* **16**, 162-170.

Boily J.-F. and Seward T. M. (2005) Palladium(II) chloride complexation: Spectrophotometric investigation in aqueous solutions from 5 to 125°C and theoretical insight into Pd-Cl and Pd-OH_2 interactions. *Geochim. Cosmochim. Acta* **69**, 3773-3789.

Boily J.-F., Seward T. M. and Charnock J. M. (2007) The hydrolysis and precipitation of Pd(II) in 0.6 mol kg^{-1} NaCl: A potentiometric, spectrophotometric, and EXAFS study. *Geochim. Cosmochim. Acta* **71**, 4834-4845.

Boudreau A. E. (2016) The Stillwater Complex, Montana – Overview and the significance of volatiles. *Mineral. Mag.* **80**, 585-637.

Boudreau A. E., Mathez E. A. and McCallum I. S. (1986) Halogen Geochemistry of the Stillwater and Bushveld Complexes: Evidence for Transport of the Platinum-Group Elements by Cl-Rich Fluids. *J. Petrol.* **27**, 967-986.

Brown G. E., Foster A. L. and Ostergren J. D. (1999) Mineral surfaces and bioavailability of heavy metals: A molecular-scale perspective. *Proc. Natl. Acad. Sci. U.S.A.* **96**, 3388-3395.

Byrne R. H. and Kump L. R. (1993) Comment on "Speciation of aqueous palladium(II) chloride solutions using optical spectroscopies" by C.D. Tait, D. R. Janecky, and P. S. Z. Rogers. *Geochim. Cosmochim. Acta* **57**, 1151-1156.

Chen K., Walker R. J., Rudnick R. L., Gao S., Gaschnig R. M., Puchtel I. S., Tang M. and Hu Z.-C. (2016) Platinum-group element abundances and Re–Os isotopic systematics of the upper continental crust through time: Evidence from glacial diamictites. *Geochim. Cosmochim. Acta* **191**, 1-16.

Cobelo-García A., Mulyani M. E. and Schäfer J. (2021) Ultra-trace interference-free analysis of palladium in natural waters by ICP-MS after on-line matrix separation and pre-concentration. *Talanta* **232**, 122289.

Coker W. B., Dunn C. E., Hall G. E. M., Rencz A. N., DiLabio R. N. W., Spirito W. A. and Campbell J. E. (1991) The behaviour of platinum group elements in the surficial environment at Ferguson Lake, N.W.T., Rottenstone Lake, Sask. and Sudbury, Ont., Canada. *J. Geochem. Explor.* **40**, 165-192.

Colombo C., Oates C. J., Monhemius A. J. and Plant J. A. (2008) Complexation of platinum, palladium and rhodium with inorganic ligands in the environment. *Geochem.: Explor. Environ. Anal.* **8**, 91-101.

Cornell R. M. and Schwertmann U. (2003) *The Iron Oxides: Structure, Properties, Reactions, Occurences and Uses*, 2nd ed. Wiley-VCH, Weinheim, Germany.

Dannecker B. and Thiele G. (1986) Darstellung und Kristallstruktur von Palladiumoxidchlorid Pd_2OCl_2. *Z. Naturforsch* **41b**, 1363-1366.

Davis J. A. and Leckie J. O. (1978) Effect of Adsorbed Complexing Ligands on Trace Metal Uptake by Hydrous Oxides. *Environ. Sci. Technol.* **12**, 1309-1315.

Davis J. A., James R. O. and Leckie J. O. (1978) Surface Ionization and Complexation at the Oxide/Water Interface I. Computation of Electrical Double Layer Properties in Simple Electrolytes. *J. Colloid Interface Sci* **63**, 480-499.

Dockrey J., Lindsay M., Mayer K., Beckie R., Norlund K., Warren L. and Southam G. (2014) Acidic Microenvironments in Waste Rock Characterized by Neutral Drainage: Bacteria–Mineral Interactions at Sulfide Surfaces. *Minerals* **4**, 170-190.

Dzingai T., McFadzean B., Tadie M. and Becker M. (2021) Decoupling the effects of alteration on the mineralogy and flotation performance of Great Dyke PGE ores. *J. S. Afr. Inst. Min. Metall.* **121**, 475-486.

Dzombak D. A. and Morel F. M. M. (1991) *Surface Complexation Modeling: Hydrous Ferric Oxide*. John Wiley & Sons.

Evans D. M. (2002) Potential for bulk mining of oxidized platinum-group element deposits. *Appl. Earth Sci.* **111**, 81-86.

Evans D. M. and Spratt J. (2000) Platinum and palladium oxides/hydroxides from the Great Dyke, Zimbabwe, and thoughts on their stability and possible extraction. In *Applied Mineralogy* (eds. D. Rammlmair, J. Mederer and T. Oberthür). A A Balkema, Rotterdam. pp. 289-292.

Evans D. M., Buchanan D. L. and Hall G. E. M. (1994) Dispersion of platinum, palladium and gold from the Main Sulphide Zone, Great Dyke, Zimbabwe. *Trans. Instn. Min. Metall. B: Appl. Earth Sci.* **103**, B57-B67.

881 Fandeur D., Juillot F., Morin G., Olivi L., Cognigni A., Webb S. M., Ambrosi J.-P., Fritsch E.,
882 Guyot F. and Brown G. E. (2009) XANES Evidence for Oxidation of Cr(III) to Cr(VI) by
883 Mn-Oxides in a Lateritic Regolith Developed on Serpentinized Ultramafic Rocks of New
884 Caledonia. *Environ. Sci. Technol.* **43**, 7384-7390.
885 Fischer W. R. and Schwertmann U. (1975) The Formation of Hematite from Amorphous
886 Iron(III)Hydroxide. *Clays Clay Miner.* **23**, 33-37.
887 Fuchs W. A. and Rose A. W. (1974) The Geochemical Behavior of Platinum and Palladium in
888 the Weathering Cycle in the Stillwater Complex, Montana. *Econ. Geol.* **69**, 332-346.
889 Galey M. L., van der Ent A., Iqbal M. C. M. and Rajakaruna N. (2017) Ultramafic geoecology of
890 South and Southeast Asia. *Bot. Stud.* **58**, 18.
891 Gray D. J., Schorin K. H. and Butt C. R. M. (1996) Mineral associations of platinum and
892 palladium in lateritic regolith, Ora Banda Sill, Western Australia. *J. Geochem. Explor.*
893 **57**, 245-255.
894 Gustafsson J. P. (2014) Visual MINTEQ. Version 3.1. Web. https://vminteq.lwr.kth.se/.
895 Han S. C., Chang E., Zechel S., Bok F. and Zavarin M. (2023) Application of community data to
896 surface complexation modeling framework development: Iron oxide protolysis. *J. Colloid*
897 *Interface Sci* **648**, 1015-1024.
898 He X., Sharma N., Stagg O., Flynn E. D., Catalano J. G. and Giammar D. E. (2024) Adsorption
899 of Neodymium, Dysprosium, and Ytterbium to Goethite under Varying Aqueous
900 Chemistry Conditions. *ACS Earth Space Chem.* **8**, 1224-1235.
901 Hey P. V. (1999) The effects of weathering on the UG2 Chromitite reef of the Bushveld
902 Complex, with special reference to the platinum-group minerals. *S. Afr. J. Geol.* **102**,
903 251-260.
904 Hwang Y. S. and Lenhart J. J. (2008) The dependence of hematite site-occupancy standard state
905 triple-layer model parameters on inner-layer capacitance. *J. Colloid Interface Sci* **319**,
906 206-213.
907 Ito A., Otake T., Maulana A., Sanematsu K., Sufriadin and Sato T. (2021) Geochemical
908 constraints on the mobilization of Ni and critical metals in laterite deposits, Sulawesi,
909 Indonesia: A mass-balance approach. *Resour. Geol.* **71**, 255-282.
910 Johnston J. H. and Lewis D. G. (1983) A detailed study of the transformation of ferrihydrite to
911 hematite in an aqueous medium at 92°C. *Geochim. Cosmochim. Acta* **47**, 1823-1831.
912 Junge M., Oberthür T., Kraemer D., Melcher F., Piña R., Derrey I. T., Manyeruke T. and Strauss
913 H. (2019) Distribution of platinum-group elements in pristine and near-surface oxidized
914 Platreef ore and the variation along strike, northern Bushveld Complex, South Africa.
915 *Miner. Deposita* **54**, 885-912.
916 Kelly S. D., Hesterberg D. and Ravel B. (2008) Analysis of Soils and Minerals Using X-ray
917 Absorption Spectroscopy. In *Methods of Soil Analysis Part 5—Mineralogical Methods*
918 (eds. A. L. Ulery and L. R. Drees). Soil Science of America, Inc., Madison. pp. 387-464.
919 Kim C. S., Rytuba J. J. and Brown G. E. (2004) EXAFS study of mercury(II) sorption to Fe- and
920 Al-(hydr)oxides. II. Effects of chloride and sulfate. *J. Colloid Interface Sci.* **270**, 9-20.
921 Koroleva L. A., Shikina N. D., Kolodina P. G., Zotov A. V., Tagirov B. R., Shvarov Y. V.,
922 Volchenkova V. A. and Shazzo Y. K. (2012) Experimental study of Pd hydrolysis in
923 aqueous solutions at 25–70°C. *Geochem. Int.* **50**, 853-859.
924 Koshcheeva I. Y., Kubrakova I. V., Korsakova N. V. and Tyutyunnik O. A. (2016) Solubility
925 and migration ability of rhodium in natural conditions: model experimental data.
926 *Geochem. Int.* **54**, 624-632.

927 Kraemer D., Junge M. and Bau M. (2017) Oxidized Ores as Future Resource for Platinum Group
928 Metals: Current State of Research. *Chem. Ing. Tech.* **89**, 53-63.
929 Kubrakova I. V., Fortygin A. V., Lobov S. G., Koshcheeva I. Y., Tyutyunnik O. A. and
930 Mironenko M. V. (2011) Migration of platinum, palladium, and gold in the water systems
931 of platinum deposits. *Geochem. Int.* **49**, 1072-1084.
932 Locmelis M., Melcher F. and Oberthür T. (2010) Platinum-group element distribution in the
933 oxidized Main Sulfide Zone, Great Dyke, Zimbabwe. *Miner. Deposita* **45**, 93-109.
934 Mann A. W. (1984) Mobility of Gold and Silver in Lateritic Weathering Profiles: Some
935 Observations from Western Australia. *Econ. Geol.* **79**, 38-49.
936 Marsh E. E. and Anderson E. D. (2011) *Ni-Co laterite deposits*. U.S. Geological Survey Open-
937 File Report 2011-1259.
938 McGregor R. G., Blowes D. W., Jambor J. L. and Robertson W. D. (1998) The solid-phase
939 controls on the mobility of heavy metals at the Copper Cliff tailings area, Sudbury,
940 Ontario, Canada. *J. Contam. Hydrol.* **33**, 247-271.
941 Molekoa M., Avtar R., Kumar P., Minh H. and Kurniawan T. (2019) Hydrogeochemical
942 Assessment of Groundwater Quality of Mokopane Area, Limpopo, South Africa Using
943 Statistical Approach. *Water* **11**, 1891.
944 Nassar N. T. and Fortier S. M. (2021) *Methodology and Technical Input for the 2021 Review and*
945 *Revision of the U.S. Critical Minerals List*. U.S. Geological Survey Open File Report
946 2021-1045.
947 Ndjigui P.-D. and Bilong P. (2010) Platinum-group elements in the serpentinite lateritic mantles
948 of the Kongo–Nkamouna ultramafic massif (Lomié region, South-East Cameroon). *J.*
949 *Geochem. Explor.* **107**, 63-76.
950 Ndjigui P.-D., Bilong P., Bitom D. and Dia A. (2008) Mobilization and redistribution of major
951 and trace elements in two weathering profiles developed on serpentinites in the Lomié
952 ultramafic complex, South-East Cameroon. *J. Afr. Earth Sci.* **50**, 305-328.
953 Newville M. (2001) IFEFFIT: interactive XAFS analysis and FEFF fitting. *J. Synchrotron Rad.*
954 **8**, 322-324.
955 Newville M. (2013) Larch: An Analysis Package for XAFS and Related Spectroscopies. *J.*
956 *Phys.: Conf. Ser.* **430**, 012007.
957 Oberthür T. (2018) The Fate of Platinum-Group Minerals in the Exogenic Environment—From
958 Sulfide Ores via Oxidized Ores into Placers: Case Studies Bushveld Complex, South
959 Africa, and Great Dyke, Zimbabwe. *Minerals* **8**, 581.
960 Oberthür T. and Melcher F. (2005) Behavior of PGE and PGM in the Supergene Environment: A
961 Case Study of Persistence and Redistribution in the Main Sulfide Zone of the Great
962 Dyke, Zimbabwe. In *Exploration for Platinum-Group Elements Deposits* (ed. J. E.
963 Mungall). Mineralogical Association of Canada. pp. 97-112.
964 Oberthür T., Weiser T. W., Gast L. and Kojonen K. (2003) Geochemistry and mineralogy of
965 platinum-group elements at Hartley Platinum Mine, Zimbabwe. *Miner. Deposita* **38**, 344-
966 355.
967 Oberthür T., Melcher F., Buchholz P. and Locmelis M. (2013) The oxidized ores of the Main
968 Sulphide Zone, Great Dyke, Zimbabwe: turning resources into minable reserves--
969 mineralogy is the key. *J. S. Afr. Inst. Min. Metall.* **113**, 191-201.
970 Oberthür T., Weiser T. W., Gast L., Wittich C. and Kojonen K. (2000) Mineralogy applied to the
971 evaluation and processing of platinum ores of the Main Sulfide Zone, Great Dyke,

Zimbabwe. In *Applied Mineralogy* (eds. D. Rammlmair, J. Mederer and T. Oberthür). A A Balkema, Rotterdam. pp. 379-382.
Oppermann L., Junge M., Schuth S., Holtz F., Schwarz-Schampera U. and Sauheitl L. (2017) Mobility and distribution of palladium and platinum in soils above Lower and Middle Group chromitites of the western Bushveld Complex, South Africa. *S. Afr. J. Geol.* **120**, 511-524.
Parker A. P., Clay P. L., Boudreau A. E., Burgess R. and O'Driscoll B. (2022) Magmatic volatiles and platinum-group element mineralization in the Stillwater layered intrusion, U.S.A. *Am. Mineral.* **107**, 797-814.
Pašava J. (1993) Anoxic sediments—an important environment for PGE; An overview. *Ore Geol. Rev.* **8**, 425-445.
Rai D., Yui M. and Kitamura A. (2012) Thermodynamic Model for Amorphous $Pd(OH)_2$ Solubility in the Aqueous Na^+–K^+–H^+–OH^-–Cl^-–ClO_4^-–H_2O System at 25°C: A Critical Review. *J. Solution Chem.* **41**, 1965-1985.
Schwertmann U. and Cornell R. M. (2000) *Iron Oxides in the Laboratory: Preparation and Characterization*, 2 ed. Wiley-VCH, Weinheim.
Sefako R., Sibanda V. and Sekgarametso K. (2019) PGM extraction from oxidized ores using flotation and leaching. *J. S. Afr. Inst. Min. Metall.* **119**, 929-936.
Stribrny B., Wellmer F.-W., Burgath K.-P., Oberthür T., Tarkian M. and Pfeiffer T. (2000) Unconventional PGE occurences and PGE mineralization in the Great Dyke: metallogenic and economic aspects. *Miner. Deposita* **35**, 260-281.
Stumm W., Huang C. P. and Jenkins S. R. (1970) Specific Chemical Interaction Affecting the Stability of Dispersed Systems. *Croat. Chem. Acts* **42**, 223-245.
Suárez S., Prichard H. M., Velasco F., Fisher P. C. and McDonald I. (2010) Alteration of platinum-group minerals and dispersion of platinum-group elements during progressive weathering of the Aguablanca Ni–Cu deposit, SW Spain. *Miner. Deposita* **45**, 331-350.
Sverjensky D. A. (2003) Standard states for the activities of mineral surface sites and species. *Geochim. Cosmochim. Acta* **67**, 17-28.
Sverjensky D. A. (2006) Prediction of the speciation of alkaline earths adsorbed on mineral surfaces in salt solutions. *Geochim. Cosmochim. Acta* **70**, 2427-2453.
Tait C. D., Janecky D. R. and Rogers P. S. Z. (1991) Speciation of aqueous palladium(II) chloride solutions using optical spectroscopies. *Geochim. Cosmochim. Acta* **55**, 1253-1264.
Takahashi Y., Minai Y., Ambe S., Makide Y. and Ambe F. (1999) Comparison of adsorption behavior of multiple inorganic ions on kaolinite and silica in the presence of humic acid using the multitracer technique. *Geochim. Cosmochim. Acta* **63**, 815-836.
Tanaka K., Tanaka M., Watanabe N., Tokunaga K. and Takahashi Y. (2017) Ligand exchange adsorption and coordination structure of Pd on δ-MnO_2 in NaCl solution. *Chem. Geol.* **460**, 130-137.
Thompson R. C. and Rodgers K. A. (1977) Laterization of the Ultramafic-Gabbro Association at North Cape, Northernmost New Zealand. *J. R. Soc. N. Z.* **7**, 347-377.
Torrent J., Guzman R. and Parra M. A. (1982) Influence of Relative Humidity on the Crystallization of Fe(III) Oxides from Ferrihydrite. *Clays Clay Miner.* **30**, 337-340.
Traoré D., Beauvais A., Augé T., Chabaux F., Parisot J. C., Cathelineau M., Peiffert C. and Colin F. (2006) Platinum and palladium mobility in supergene environment: The residual origin of the Pirogues River mineralization, New Caledonia. *J. Geochem. Explor.* **88**, 350-354.

Tyutyunnik O. A., Kubrakova I. V. and Pryazhnikov D. V. (2016) Formation and sorption behavior of the palladium thiosulfate complexes under natural conditions (model experiments). *Geochem. Int.* **54**, 85-91.

Uheida A., Iglesias M., Fontas C., Hidalgo M., Salvado V., Zhang Y. and Muhammed M. (2006) Sorption of palladium(II), rhodium(III), and platinum(IV) on Fe_3O_4 nanoparticles. *J. Colloid Interface Sci.* **301**, 402-408.

van der Ent A., Cardace D., Tibbett M. and Echevarria G. (2018) Ecological implications of pedogenesis and geochemistry of ultramafic soils in Kinabalu Park (Malaysia). *Catena* **160**, 154-169.

Van Middlesworth J. M. and Wood S. A. (1999) The stability of palladium(II) hydroxide and hydroxy-chloride complexes: An experimental solubility study at 25-85°C and 1 bar. *Geochimica et Cosmochimica Acta* **63**, 1751-1765.

Violante A., Cozzolino V., Perelomov L., Caporale A. G. and Pigna M. (2010) Mobility and Bioavailability of Heavy Metals and Metalloids in Soil Environments. *J. Soil Sci. Plant Nutr.* **10**, 268-292.

Webb S. M. (2005) SIXpack: a graphical user interface for XAS analysis using IFEFFIT. *Phys. Scr.* **T115**, 1011-1014.

Wilde A. (2005) Descriptive Ore Deposit Models: Hydrothermal & Supergene Pt & Pd Deposits. In *Exploration for Platinum-Group Elements Deposits* (ed. J. E. Mungall). Mineralogical Association of Canada. pp. 145-161.

Willmore C. C., Boudreau A. E. and Kruger F. J. (2000) The Halogen Geochemistry of the Bushveld Complex, Republic of South Africa: Implications for Chalcophile Element Distribution in the Lower and Critical Zones. *J. Petrol.* **41**, 1517-1539.

Wood S. A., Mountain B. M. and Fenlon B. J. (1989) Thermodynamic Constraints on the Solubility of Platinum and Palladium in Hydrothermal Solutions: Reassessment of Hydroxide, Bisulfide, and Ammonia Complexing. *Econ. Geol.* **84**, 2020-2028.

Wood S. A., Mountain B. M. and Pan P. (1992) The Aqueous Geochemistry of Platinum, Palladium, and Gold: Recent Experimental Constraints and a Re-evaluation of Theoretical Predictions. *Canad. Mineral.* **30**, 955-982.

Wood S. A., Tait C. D., Vlassopoulos D. and Janecky D. R. (1994) Solubility and spectroscopic studies of the interaction of palladium with simple carboxylic acids and fulvic acid at low temperature. *Geochim. Cosmochim. Acta* **58**, 625-637.

Zientek M. L., Loferski P. J., Parks H. L., Schulte R. F. and Seal R. R., II (2017) Platinum-group elements. In *Critical Mineral Resources of the United States—Economic and Environmental Geology and Prospects for Future Supply* (eds. K. J. Schulz, J. H. DeYoung, Jr., R. R. Seal, II and D. C. Bradley). U.S. Department of the Interior, U.S. Geological Survey.

Tables

Table 1. Langmuir parameters from isotherms fit to the uptake data for the hematite and 2-line ferrihydrite experiments at pH 4±0.1.

Mineral	[Cl] (mM)[a]	K (uM^{-1})[b]	Γ_{max} (µmol/m^2)[c]
Hematite	0.47 ± 0.02	0.29 ± 0.03[d]	1.3[e]
	2.2 ± 0.4	0.100 ± 0.003	1.3
	4.9 ± 0.4	0.038 ± 0.003	1.30 ± 0.04
	9.7 ± 0.3	0.017 ± 0.002	1.30 ± 0.04
2-line ferrihydrite	0.48 ± 0.01	0.38 ± 0.06	4.2 ± 0.3
	1.85 ± 0.02	0.14 ± 0.02	4.8 ± 0.2
	9.87 ± 0.01	0.023 ± 0.003	4.4 ± 0.2

[a]Chloride is reported as the average final aqueous concentration in experimental samples, plus or minus 1 standard deviation.
[b]K is an affinity constant that represents the favorability of adsorption.
[c]Γ_{max} is the maximum surface area-normalized binding capacity
[d]Uncertainties in K and Γ_{max} are reported as 1σ.
[e]Γ_{max} for the two lowest chloride conditions for hematite was fixed during fitting

Table 2. Measured zeta potential for hematite and 2-line ferrihydrite at pH 4±0.1 in the presence of varying amounts of NaCl.

Mineral	NaCl (mM)	Zeta Potential (mV)
Hematite	0.5 (3)[a]	45.3 ± 0.4[b]
	2 (3)	45.1 ± 0.4
	10 (6)	49 ± 2
2-line ferrihydrite	0.5 (3)	37 ± 2
	2 (3)	36.6 ± 0.8
	10 (6)	35 ± 1

[a]The number in parentheses reports the number of measurements collected from the same sample.
[b]Zeta potential is reported as the average, plus or minus one standard deviation, of multiple measurements.

Table 3. Pd K-edge EXAFS Fitting Parameters.

Sample[a]	[Cl] (mM)	Adsorbed Pd (μmol/m²)[b]	Path	CN[c]	R (Å)[d]	σ² (Å²)[e]	ΔE₀ (eV)[f]	*R* factor[g]	χ_v^{2g}
H0.5h	0.43	0.50	Pd-O	2.1(1)[h]	2.012(9)	0.0027(4)	5(1)	0.013	23.9
			Pd-Cl	1.9	2.293(6)	0.0027			
			Pd-Fe1	0.3(1)	2.91(3)	0.003(2)			
			Pd-Fe2	0.4(1)	3.07(3)	0.003			
			Pd-Fe3	0.3	3.68(3)	0.003			
H5h	4.7	0.88	Pd-O	1.7(1)	2.01(1)	0.0020(4)	6(1)	0.015	45.0
			Pd-Cl	2.3	2.297(5)	0.0020			
			Pd-Fe1	0.2(2)	2.92(7)	0.004(3)			
			Pd-Fe2	0.3(2)	3.10(6)	0.004			
			Pd-Fe3	0.5	3.65(4)	0.004			
H10l	9.7	0.29	Pd-O	1.5(1)	2.014(9)	0.0022(4)	6.3(8)	0.008	19.3
			Pd-Cl	2.5	2.298(4)	0.0022			
			Pd-Fe1	0.2(1)	2.92(5)	0.005(2)			
			Pd-Fe2	0.4(1)	3.12(4)	0.005			
			Pd-Fe3	0.4	3.67(3)	0.005			
H10h	10	1.1	Pd-O	1.4(2)	2.02(2)	0.0025(4)	7(1)	0.011	63.5
			Pd-Cl	2.6	2.303(5)	0.0025			
			Pd-Fe1	0.4(1)	2.93(2)	0.002(2)			
			Pd-Fe2	0.3(1)	3.11(3)	0.002			
			Pd-Fe3	0.3	3.61(3)	0.002			
F0.5h	0.43	1.4	Pd-O	2.72(6)	2.012(5)	0.0021(3)	6.3(9)	0.012	14.8
			Pd-Cl	1.28	2.291(5)	0.0021			
			Pd-Fe1	0.5(1)	2.95(2)	0.004(2)			
			Pd-Fe2	0.3(1)	3.15(3)	0.004			
			Pd-Fe3	0.2	3.63(8)	0.004			
F2h	1.6	2.6	Pd-O	2.14(7)	2.012(6)	0.0018(3)	5.9(7)	0.007	24.4
			Pd-Cl	1.86	2.289(4)	0.0018			
			Pd-Fe1	0.36(6)	2.94(2)	0.002(1)			
			Pd-Fe2	0.29(7)	3.10(2)	0.002			
			Pd-Fe3	0.35	3.61(2)	0.002			
F10h	8.9	2.8	Pd-O	1.83(10)	2.014(8)	0.0017(3)	6.1(9)	0.009	30.0
			Pd-Cl	2.17	2.293(4)	0.0017			
			Pd-Fe1	0.33(8)	2.94(3)	0.002(2)			
			Pd-Fe2	0.35(9)	3.10(3)	0.002			
			Pd-Fe3	0.32	3.62(2)	0.002			

[a]Sample names that start with "H" were hematite samples; Names that start with "F" were 2-line ferrihydrite samples.
[b]Estimated by measuring aqueous Pd remaining and calculating adsorbed Pd using Langmuir isotherm values.
[c]Coordination number.
[d]Interatomic distance.
[e]Debye-Waller factor.
[f]Energy shift parameter.
[g]Goodness-of-fit parameters (Kelly et al., 2008)
[h]The estimated standard deviations as errors in the last digit are given in parentheses. Parameters that were constrained during fitting are listed with no uncertainties.

Table 4. Surface reactions used for surface complexation modeling.

No.	Reaction	Log K	Source
1	$>FeOH + H^+ \rightleftharpoons >FeOH_2^+$	7.60	Han et al. (2023)
2	$>FeOH \rightleftharpoons >FeO^- + H^+$	-9.20	
3	$2>FeOH + Pd^{2+} + Cl^- \rightleftharpoons (>FeO)_2PdCl^- + 2H^+$	-0.07	This study
4	$2>FeOH + Pd^{2+} + 2Cl^- + H^+ \rightleftharpoons (>FeOH_2)(>FeOH)PdCl_2^+$	21.19	
5	$>FeOH + Pd^{2+} + 3Cl^- \rightleftharpoons >FeOHPdCl_3^-$	11.66	

Figures

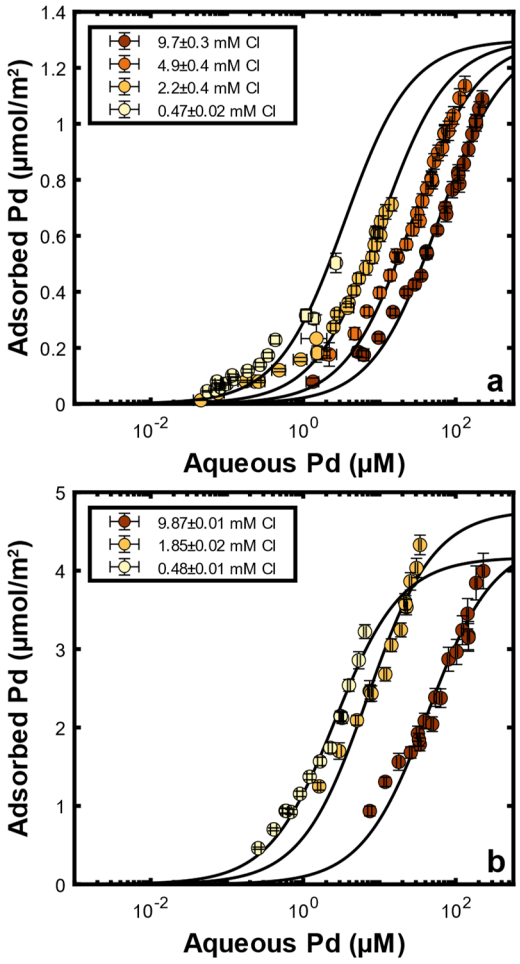

Figure 1. Pd adsorption to hematite (a) or 2-line ferrihydrite (b) at pH 4±0.1 compared to the final measured dissolved Pd at multiple different total chloride concentrations. Corresponding single Langmuir isotherms are shown as lines.

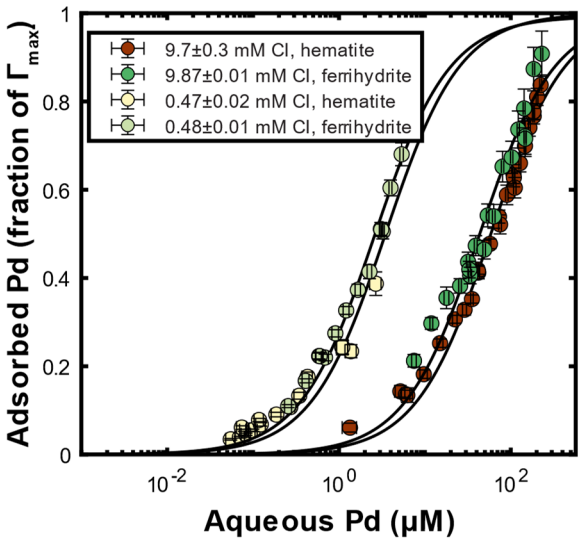

Figure 2. Pd adsorption to hematite and 2-line ferrihydrite at pH 4±0.1 (normalized to the calculated maximum binding capacity given in **Table 1**) compared to the final measured dissolved Pd in the presence of approximately 10 mM chloride. Single Langmuir isotherms are shown as lines.

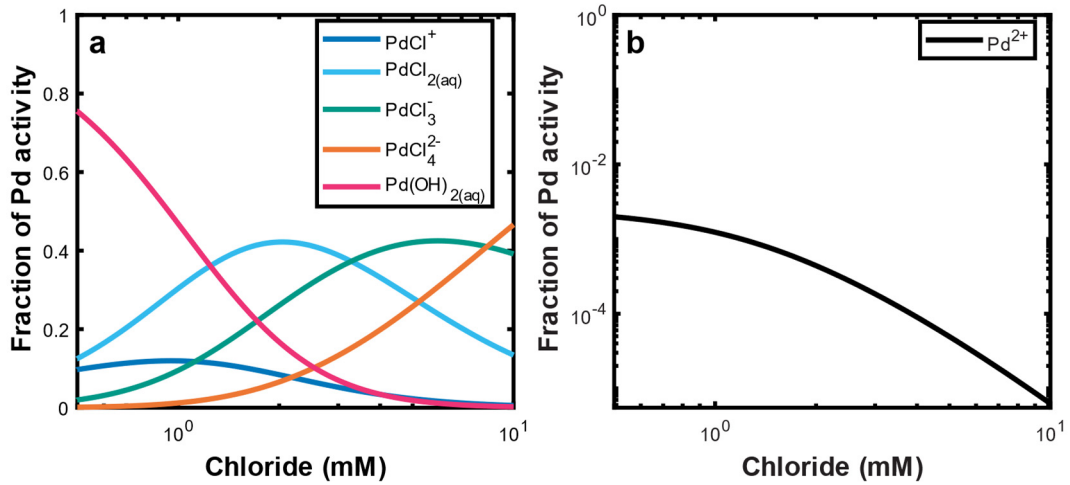

Figure 3. The relative activities of major Pd species (a) and Pd^{2+} (b) at pH 4 as a function of increasing chloride from 0.5 to 10 mM.

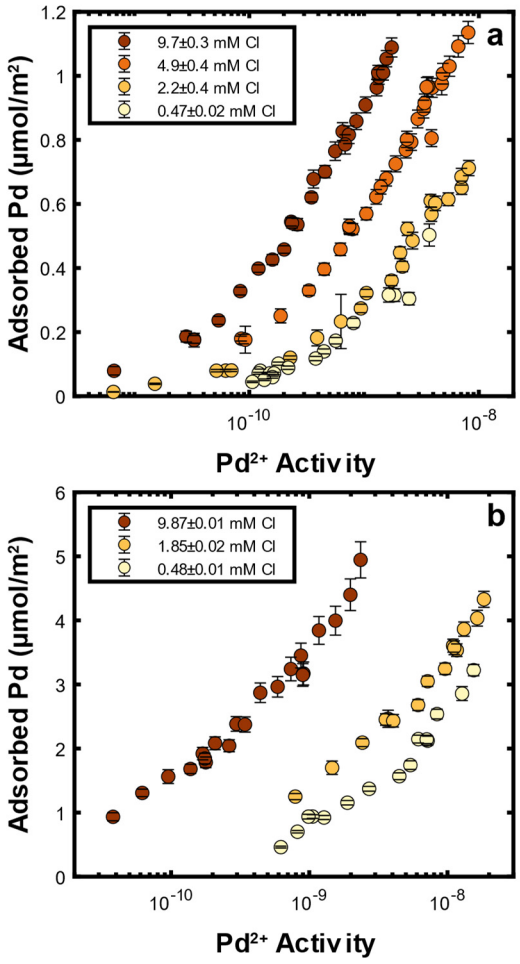

Figure 4. Pd adsorption to hematite (a) and 2-line ferrihydrite (b) at pH 4±0.1, compared to the calculated activity of Pd^{2+} at multiple different total chloride concentrations. The experimental errors for adsorbed Pd are shown.

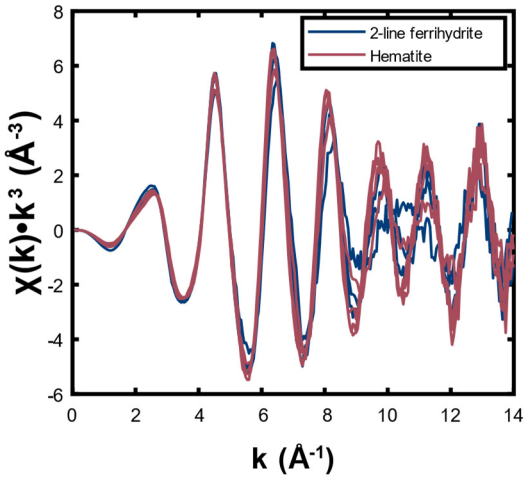

Figure 5. Pd K-edge spectra of 2-line ferrihydrite and hematite.

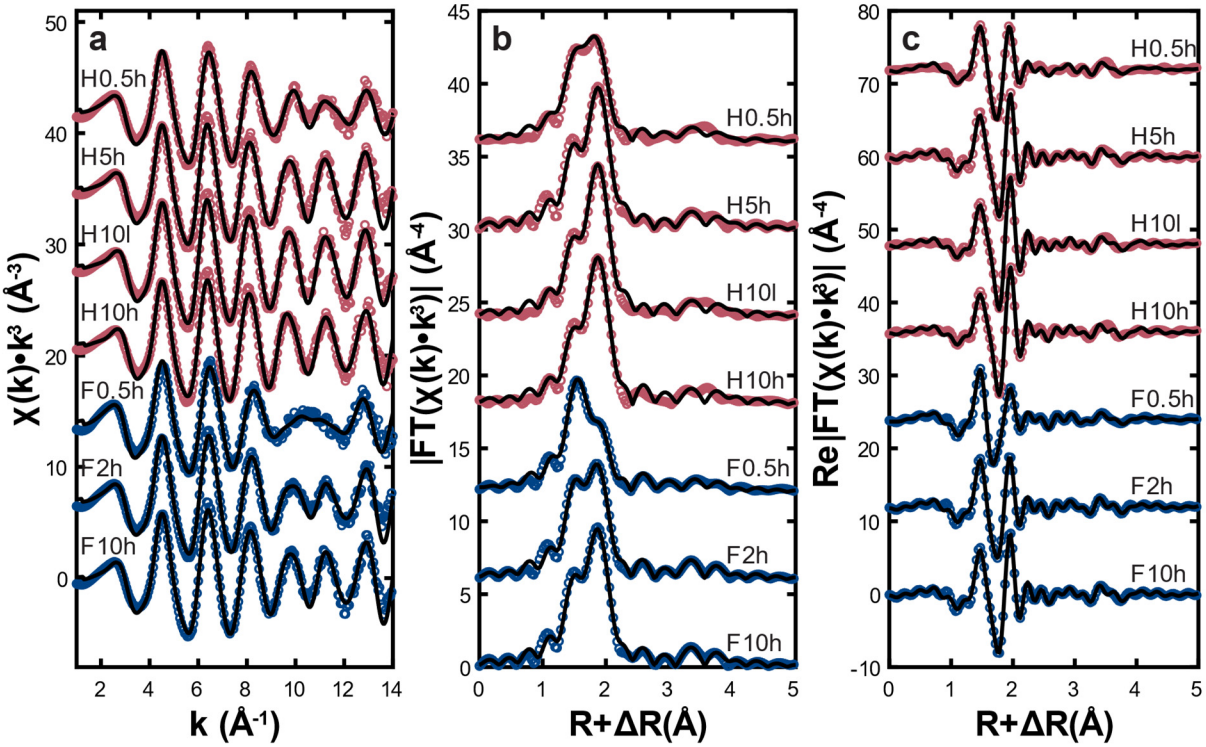

Figure 6. Data (symbols) and structural model fit (solid line) to the Pd K-edge spectra (a), Fourier transform magnitudes (b), and real components of the Fourier transforms (c). Detailed sample information is provided in **Tables 3** and **S4**.

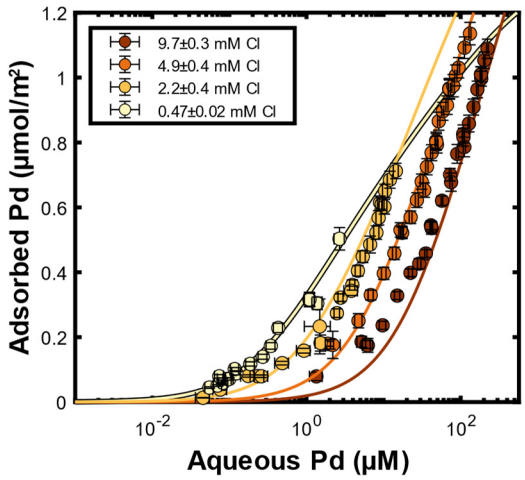

Figure 7. Surface complexation model of Pd adsorbed to hematite under varying chloride concentrations at pH 4±0.1 Experimental data are shown as symbols and model-generated total calculated adsorption as lines. Speciation of adsorbed Pd predicted by the model is provided in **Figure S4**.

Supplementary Material for:

Competitive and Cooperative Effects of Chloride on Palladium(II) Adsorption to Iron (Oxyhydr)oxides: Implications for Mobility During Weathering

Emily G. Wright[1], Xicheng He[2], Elaine D. Flynn[1], Daniel E. Giammar[2], Jeffrey G. Catalano[1*]

1. Department of Earth, Environmental, and Planetary Sciences, Washington University in St. Louis, Saint Louis, MO 63130, USA
2. Department of Energy, Environmental, and Chemical Engineering, Washington University in St. Louis, Saint Louis, MO 63130, USA

*Corresponding author: catalano@wustl.edu

Mineral Characterization

Minerals were synthesized as described in the main text. A subsample of each mineral suspension was dried for characterization. Hematite samples were dried overnight at 70°C. Batch F1 was dried overnight at 40°C. Batch F2 was freeze-dried. An unground portion of the dried subsample was used for BET specific surface area measurements (**Table S1**), which were collected with a Quantachrome Nova 2000e instrument. Prior to analysis, samples were degassed under vacuum at 100°C (hematite) or 23°C (2-line ferrihydrite) for at least 18 hours. X-ray diffraction (XRD) patterns were collected with a Bruker d8 Advance Diffractometer using Cu Kα radiation to ensure no other mineral phases were present (**Fig. S1**). For most batches, XRD pattern collection conditions were the same: 10-90° 2θ, 0.02° step size, and 0.2 second count time. However, the XRD pattern of H1 was collected with a 0.5 second count time and the XRD pattern of H2 was collected with a 0.5 second count time over the range of 10 to 75° 2θ. We did not observe any additional peaks in all but one of the collected XRD patterns. For batch H4, we did observe an additional small peak around ~18° 2θ, which is consistent with polytetrafluoroethylene (PTFE). While all other batches were subsampled and dried shortly after synthesis, a portion of batch H4 was not dried until several weeks after synthesis, resulting in the

presence of PTFE from rubbing of the PTFE-coated stir bar against the bottom of the bottle in which the suspension was stored.

Pd Adsorption to Hematite at pH 3

We performed an additional macroscopic binding experiment at lower pH to provide a comparison for predictions from the surface complexation model. Following the same procedures as described in **Section 2.2**, solutions of 10 mL total volume containing 10 to 350 μM dissolved Pd were reacted with 1 g/L hematite in approximately 10 mM total chloride at pH 3±0.05 for 24 hours. The pH was measured with our chloride-free setup (described in **Section 2.2**) to prevent the addition of excess chloride. At the end of the experiment, the samples were processed in the same manner as the pH 4 samples.

We found that at the same aqueous chloride concentration, decreasing pH resulted in less Pd adsorption (**Fig. S2**). Based on our Langmuir isotherm fit, this is due to both a decrease in the surface area-normalized binding capacity and the adsorption affinity (**Table S2**). However, the slight decrease in binding capacity may be due to differences between batches of hematite used (**Table S1**).

Table S1. Details about mineral batches used for various experimental samples.

Batch Name	Mineral[a]	Measured Surface Area (m^2/g)[b]	Corresponding Experiments
H1	hematite	n.a.[c]	EXAFS sample H10h
H2	hematite	24.7	5 and 10 mM Cl experiments at pH 4
H3	hematite	23.8	0.5 and 2 mM Cl experiments at pH 4
H4	hematite	n.a.[c]	EXAFS samples H0.5h, H5h, H10l; zeta potential measurements
H5	hematite	23.9	10 mM Cl experiment at pH 3
F1[d]	2-line ferrihydrite	133	0.5, 2, and 10 mM Cl experiments at pH 4
F2[d]	2-line ferrihydrite	94.6	EXAFS samples F0.5h, F2h, F10h; zeta potential measurements

[a]Mineralogy confirmed with XRD (see **Fig. S1**).
[b]BET specific surface area.
[c]Surface area was not measured for select mineral batches only used for EXAFS samples.
[d]Batch F1 was dried in the oven at 40°C overnight while Batch F2 was freeze-dried for XRD and surface area measurements.

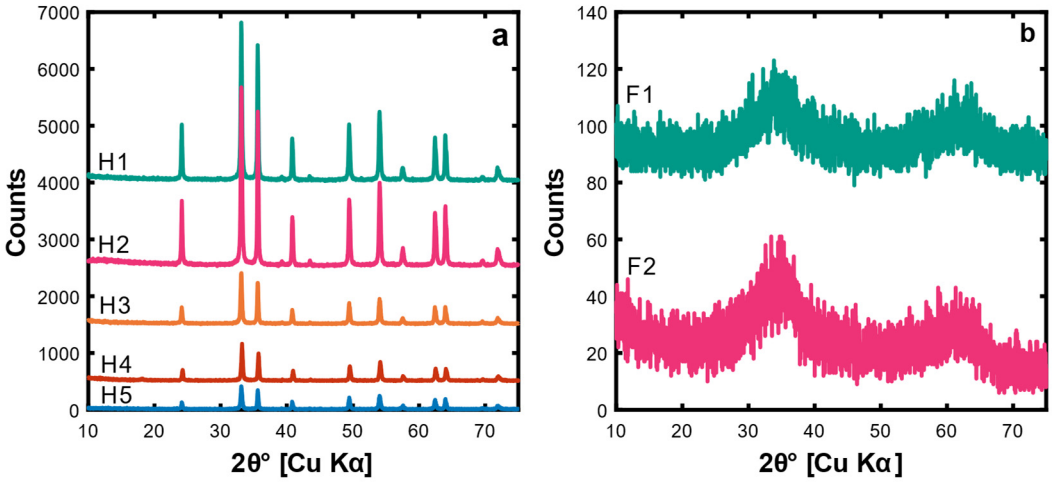

Figure S1. X-ray diffraction patterns of synthesized hematite (a) and 2-line ferrihydrite (b) batches used in study. The variations in hematite line intensity reflect differences in sample packing.

Table S2. Single Langmuir parameters from isotherms fit to the uptake data for the hematite experiment conducted at pH 3.

Mineral (pH)	[Cl] (mM)[a]	K (uM^{-1})[b]	Γ_{max} ($\mu mol/m^2$)[c]
Hematite (3±0.05)	9.84 ± 0.08	0.008 ± 0.002[d]	1.1 ± 0.1

[a]Chloride is reported as the average final aqueous concentration in experimental samples, plus or minus 1 standard deviation.
[b]K is an affinity constant that represents the favorability of adsorption.
[c]Γ_{max} is the maximum surface area-normalized binding capacity
[d]Uncertainties in K and Γ_{max} are reported as 1σ.

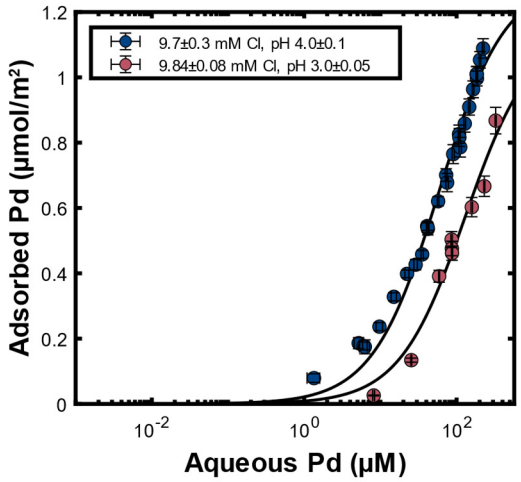

Figure S2. Pd adsorption to hematite at approximately 10 mM Cl compared to the final measured dissolved Pd at pH 3±0.05 and pH 4±0.1. Corresponding single Langmuir isotherms are shown as lines.

Table S3. Equilibrium constants for Pd complexation reactions used in the study, from Rai et al. (2012)

Reaction	log K°
$Pd(OH)_{2(aq)} + 2H^+ \rightleftharpoons 2H_2O + Pd^{2+}$	5.42
$Pd(OH)_3^- + 3H^+ \rightleftharpoons 3H_2O + Pd^{2+}$	15.48
$PdCl^+ \rightleftharpoons Cl^- + Pd^{2+}$	-5
$PdCl_{2(aq)} \rightleftharpoons 2Cl^- + Pd^{2+}$	-8.42
$PdCl_3^- \rightleftharpoons 3Cl^- + Pd^{2+}$	-10.93
$PdCl_4^{2-} \rightleftharpoons 4Cl^- + Pd^{2+}$	-13.05
$PdCl_3(OH)^{2-} + H^+ \rightleftharpoons H_2O + 3Cl^- + Pd^{2+}$	-3.77

Table S4. Details about EXAFS sample experimental conditions.

Sample	Mineral Batch	Mineral Loading (g/L)	Sample Volume (mL)	Aqueous Chloride (mM)	Final Aqueous Pd (µM)	Adsorbed Pd (µmol/m²)[a]
H0.5h	H4	2	100	0.43	17.2	0.50
H5h	H4	4	50	4.7	55.7	0.88
H10l	H4	4	50	9.7	2.18	0.29
H10h	H1	1	100	10	273	1.1
F0.5h	F2	0.1	100	0.43	1.27	1.4
F2h	F2	0.4	100	1.6	8.30	2.6
F10h	F2	0.8	100	8.9	75.7	2.8

[a]Adsorbed Pd (µmol/m²) was estimated by measuring final aqueous Pd and calculating the theoretical equilibrium adsorbed Pd predicted by the Langmuir isotherms (**Table 1**) fit to our macroscopic binding data.

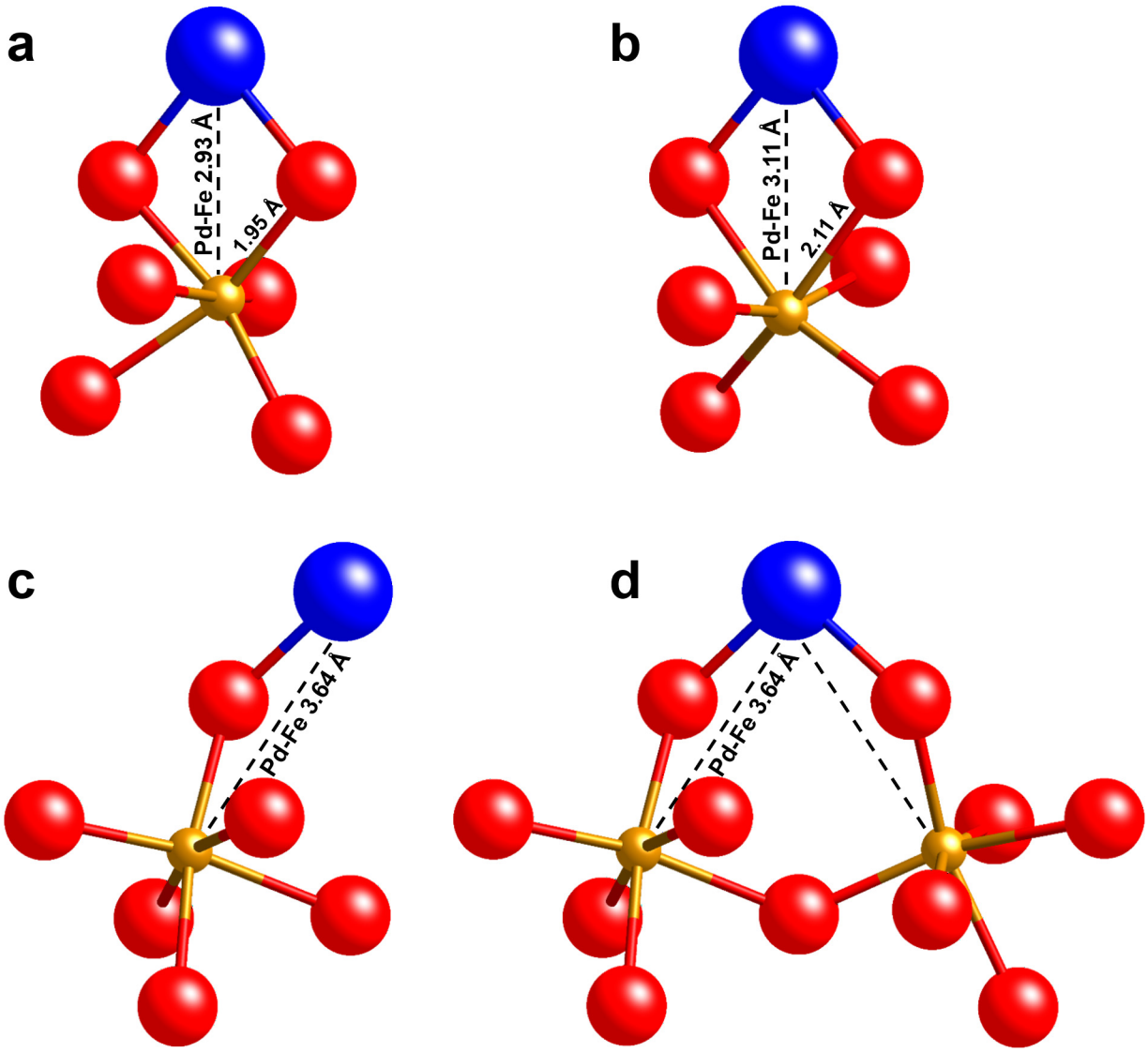

Figure S3. Potential binding geometries for Pd surface complexes consistent with EXAFS results and the coordination of octahedra in hematite: (a) edge-sharing bidentate complex with short Pd-Fe distance; (b) edge-sharing bidentate complex with a long Pd-Fe distance; (c) monodentate complex; (d) bridging bidentate complex. All Pd-O bond lengths are 2.01 Å. Both Fe-O bond lengths for the surface oxygens coordinating to Pd are the same in (a) and (b). Fe-O bond lengths in (c) and (d) are 1.95 Å, but similar Pd-Fe distances are possible for 2.11 Å Fe-O bonds with some lateral shifts in atom positions.

Table S5. Principal component analysis results for the EXAFS spectra of Pd adsorbed to ferrihydrite and hematite.

Component	Variance	Cumulative Variance	IND
1	0.946970	0.946970	0.01763
2	0.041028	0.987998	0.00461
3	0.005522	0.993521	0.00492
4	0.002930	0.996451	0.00658
5	0.001618	0.998069	0.01197
6	0.001189	0.999258	0.03329
7	0.000742	1.000000	-

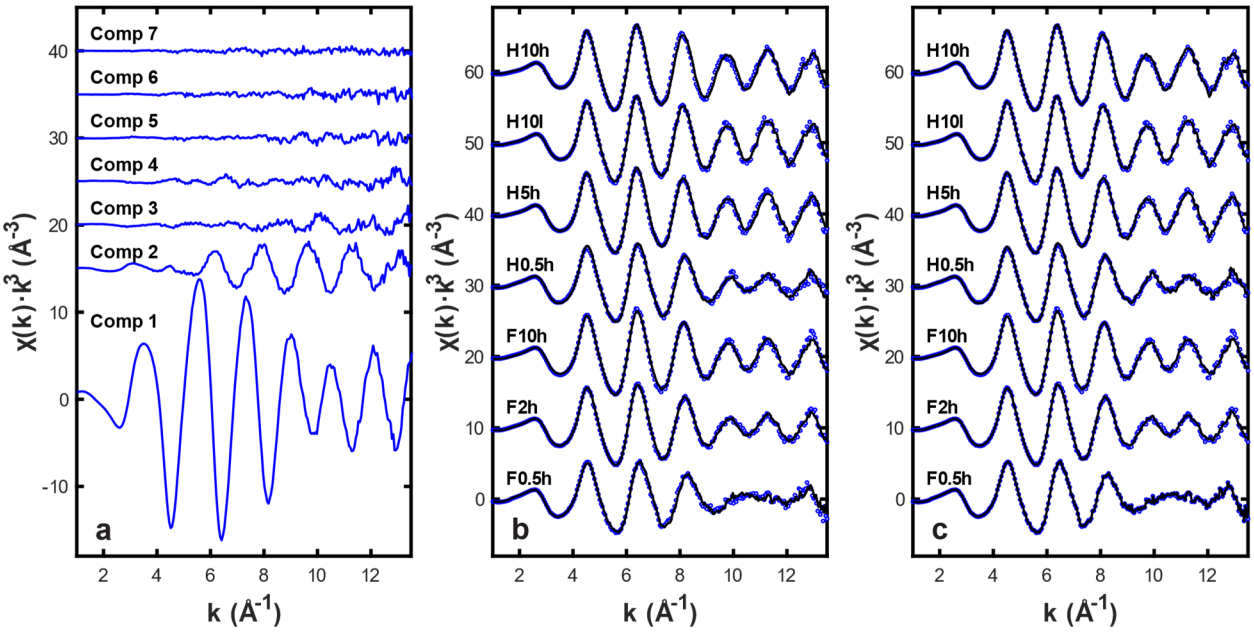

Figure S4. Results of principal component analysis of the EXAFS spectra of Pd adsorbed to hematite and ferrihydrite. (a) Principal components derived from analysis. (b) Reconstruction of the experimental spectra using two principal components. (c) Reconstruction of the experimental spectra using three principal components. Detailed sample information can be found in **Table S4**.

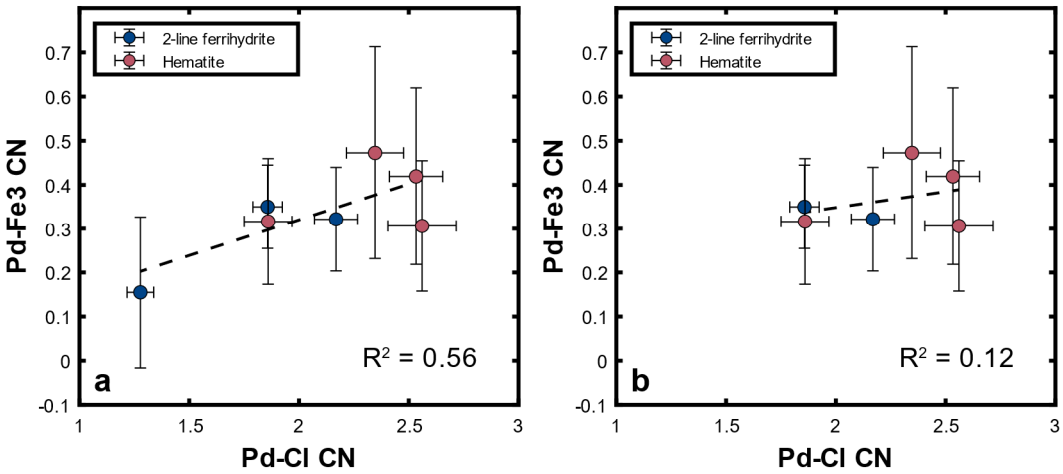

Figure S5. The coordination numbers (CN) for the Pd-Fe3 path versus the Pd-Cl path for the structural model fits to our EXAFS spectra (see **Table 3**). An unweighted linear regression line and associated R^2 value are shown for (a) all EXAFS samples and (b) all EXAFS samples excluding sample F0.5h. The errors for the Pd-Cl path are taken from the errors for the associated Pd-O path. The errors for the Pd-Fe3 path are calculated as the square root of the sum of the squared errors for the Pd-Fe1 and Pd-Fe2 paths.

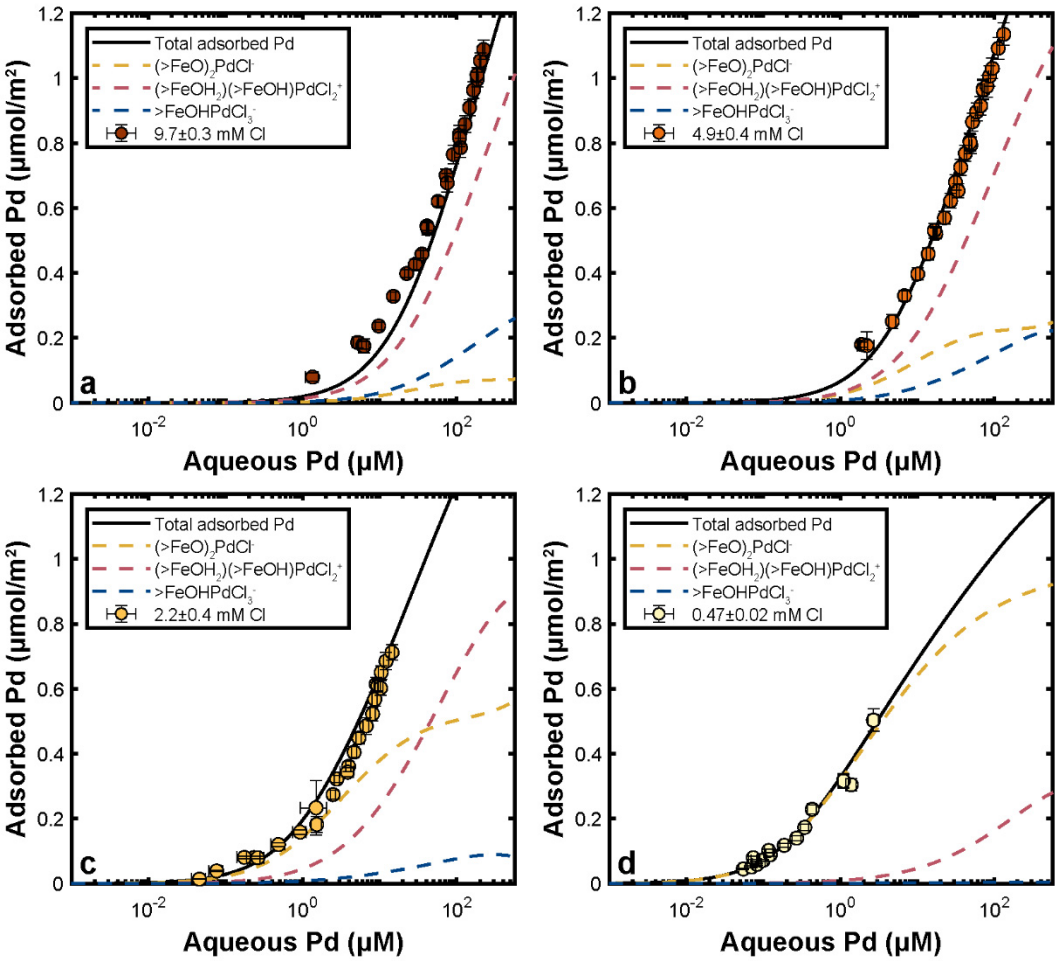

Figure S6. Speciation of adsorbed Pd predicted by the surface complexation model with (a) 10 mM, (b) 5 mM, (c) 2 mM, and (d) 0.5 mM chloride for experiments conducted at pH 4±0.1. Experimental data are shown as symbols and model-generated calculated adsorption (overall predicted adsorption and contributions of specific surface complexes) as lines.

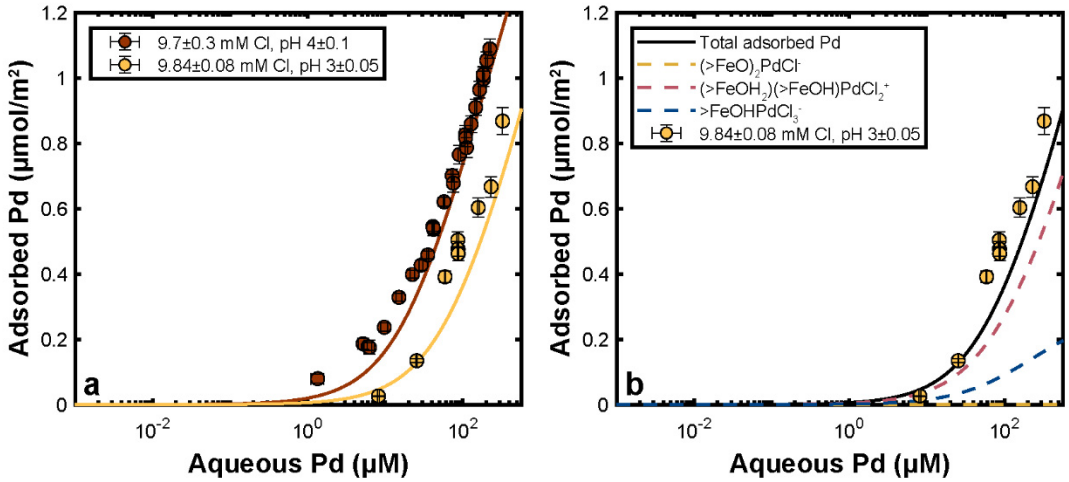

Figure S7. (a) Surface complexation model for Pd adsorption with approximately 10 mM chloride at pH 3 and 4. (b) Model predicted speciation of adsorbed Pd at pH 3±0.05. Experimental data are shown as symbols and model-generated total calculated adsorption (a) or overall predicted adsorbed Pd and the contribution of specific Pd surface complexes (b) as lines.

References Cited

Rai D., Yui M. and Kitamura A. (2012) Thermodynamic Model for Amorphous $Pd(OH)_2$ Solubility in the Aqueous Na^+–K^+–H^+–OH^-–Cl^-–ClO_4^-–H_2O System at 25°C: A Critical Review. *J. Solution Chem.* **41**, 1965-1985.